Materials Today Bio 22 (2023) 100740

Contents lists available at ScienceDirect

Materials Today Bio

journal homepage: www.journals.elsevier.com/materials-today-bio

Physical stimuli-emitting scaffolds: The role of piezoelectricity in tissue regeneration

Carmen Alvarez-Lorenzo [a,*], Mariana Zarur [a], Alejandro Seijo-Rabina [a], Barbara Blanco-Fernandez [a], Isabel Rodríguez-Moldes [b], Angel Concheiro [a]

[a] Departamento de Farmacología, Farmacia y Tecnología Farmacéutica, I+D Farma (GI-1645), Facultad de Farmacia, Instituto de Materiales (iMATUS) and Health Research Institute of Santiago de Compostela (IDIS), Universidade de Santiago de Compostela, 15782, Santiago de Compostela, Spain
[b] Grupo NEURODEVO, Departamento de Bioloxía Funcional, Universidade de Santiago de Compostela, 15782, Santiago de Compostela, Spain

ARTICLE INFO

Keywords:
Piezostimulation
Electroactive scaffolds
Bone
Cartilage
wound healing
Electrospinning
3D printing

ABSTRACT

The imbalance between life expectancy and quality of life is increasing due to the raising prevalence of chronic diseases. Musculoskeletal disorders and chronic wounds affect a growing percentage of people and demand more efficient tools for regenerative medicine. Scaffolds that can better mimic the natural physical stimuli that tissues receive under healthy conditions and during healing may significantly aid the regeneration process. Shape, mechanical properties, pore size and interconnectivity have already been demonstrated to be relevant scaffold features that can determine cell adhesion and differentiation. Much less attention has been paid to scaffolds that can deliver more dynamic physical stimuli, such as electrical signals. Recent developments in the precise measurement of electrical fields *in vivo* have revealed their key role in cell movement (galvanotaxis), growth, activation of secondary cascades, and differentiation to different lineages in a variety of tissues, not just neural. Piezoelectric scaffolds can mimic the natural bioelectric potentials and gradients in an autonomous way by generating the electric stimuli themselves when subjected to mechanical loads or, if the patient or the tissue lacks mobility, ultrasound irradiation. This review provides an analysis on endogenous bioelectrical signals, recent developments on piezoelectric scaffolds for bone, cartilage, tendon and nerve regeneration, and their main outcomes *in vivo*. Wound healing with piezoelectric dressings is addressed in the last section with relevant examples of performance in animal models. Results evidence that a fine adjustment of material composition and processing (electrospinning, corona poling, 3D printing, annealing) provides scaffolds that act as true emitters of electrical stimuli that activate endogenous signaling pathways for more efficient and long-term tissue repair.

1. Introduction

Improvements in nutrition and health programs throughout the 20th century have resulted in a very considerable increase in life expectancy [1]. The population that is over 60 years of age, and even 80 years of age, is increasingly relevant [2]. However, the increase in life expectancy does not run parallel to the quality of life. The United Nations reports highlight the paradox of that an extension of life expectancy is accompanied by a cumulative reduction in quality of life due to the increasing prevalence of degenerative diseases that cause disability. In developed countries, the sum of all the hours of disability from the age of 60 causes a loss of about 9 years of quality of life [3]. Therefore, health actions have the additional challenge of trying to delay or mitigate disability problems. Although there are small differences between women and men (gender determines the incidence), most pathologies affect the musculoskeletal tissue (back and neck pain, and osteoarthritis), are associated with diabetes, or have to do with vision problems or with some types of cancer [4].

Pathologies of the musculoskeletal tissue affect the mobility, independence, and quality of life of more than 100 million people in Europe and 125 million people in the United States, with similar rates (approximately three out of four people over 65 years) observed in other countries [5]. The incidence of musculoskeletal disorders is greater than the sum of chronic cardiovascular and respiratory pathologies. For the latter two, the advances in pharmacological treatments make it possible to regulate the manifestation of the symptoms and disease progression through controlling cholesterol levels, blood pressure, blood glucose, or bronchodilation, among other medications. On the contrary, there are no similar tools available to control the pain and progression of

* Corresponding author.
E-mail address: carmen.alvarez.lorenzo@usc.es (C. Alvarez-Lorenzo).

https://doi.org/10.1016/j.mtbio.2023.100740
Received 19 May 2023; Received in revised form 1 July 2023; Accepted 19 July 2023
Available online 20 July 2023

Abbreviations list

AF	annulus fibrosus
ALP	alkaline phosphatase
bFGF	basic fibroblast growth factor
BSP	bone sialoprotein
BV	bone volume
DMP	dentin matrix protein
ECM	extracelular matrix
EGF	epidermal growth factor
FDA	Food and Drug Administration
FGF	fibroblast growth factor
FIN	flexible intramedullary nail
HA	hydroxyapatite
HIF-1 α	hypoxia-inducible factor 1 α
Hsp90	heat shock protein 90
MSC	mesenchymal stem cell
NGF	nerve growth factor
NP	nucleus pulposus
P(VDF-TeFE)	poly(vinylidene fluoride-tetrafluoroethylene)
P(VDF-TrFE)	poly(vinylidene fluoride-tri-fluoroethylene)
PCL:	poly-ε-caprolactone
PDGF	platelet derived growth factor
PDMS	polydimethylsiloxane
PDX	polydioxanone
PEDOT	poly(3,4-ethylene dioxythiophene)
PFM	Piezoresponse Force Microscopy
PHBV	poly(hydroxybutyrate-co-valerate)
PLLA	poly-L-lactic acid
PU	polyurethane
PVA	polyvinyl alcohol
PVDF	polyvinylidene fluoride
ROS	reactive oxygen species
TBAC	tetrabutylammonium chloride
TGF-β1	transforming growth factor beta 1
Treg	regulatory T cells
TV	total volume fraction
US	ultrasound
VEGF	vascular epithelial growth factor
Vm	membrane potential
WED	wireless electroceutical dressing

disability associated with diseases that affect bone, tendon and cartilage. In particular, there are relevant clinical needs related to: critical bone defects, i.e., lesions larger than those the body can regenerate by itself, which may originate from fractures (due to osteoporosis or trauma) or surgical resections associated with tumors and infections; osteoarthritis, still considered a degenerative disease with no cure; and severe tendon injuries, in which end-to-end repair using sutures or grafts are associated to post-surgery complications that cause a considerable burden on healthcare systems with approx. 1 million additional days of inpatient care per year [6].

The ideal material for bone reconstruction continues to be the autologous or allogeneic bone graft from donors, which has the structure and growth factors necessary for regeneration, but its availability is limited. Inert implants serve to join bone fragments but do not directly contribute to regeneration and are even an impediment in growing people. The majority of patients with large prostheses are not able to carry out their previous sports practice and it is even unknown to what extent physical exercise contributes to the deterioration of the prosthesis [7]. All of these constraints together with the limited useful life of the implant are relevant disadvantages considering the increasing life expectancy. The search for synthetic strategies to regenerate native tissue has given rise to biodegradable porous scaffolds that support cell growth, release some growth factors and then disappear as new tissue is formed. Although these scaffolds represent a considerable advance, they still exhibit poor integration, often delay vascularization and do not fulfill the main functions of the native tissue, or if they do, it is only for a limited time.

In this context, it is also worth highlighting the uncovered need for treatment of chronic wounds or ulcers, a problem exacerbated by the concomitance of immobility, diabetes and peripheral vascular disease, which can also lead to amputations compromising the lives of the patients [8]. Chronic ulcers are characterized by a chronic inflammatory state often associated with infection, which can spread to the bone. Skin regeneration demands a tiny control of enzymatic activity, the supply of growth factors, especially for neovascularization, and the prevention of biofilm formation [9].

Despite remarkable advances in the field of regenerative medicine (the Tissue Engineering discipline was coined in 1987), 35 years later very few products have reached the clinic [10,11]. In this context, it is clear that a paradigm shift is required to address tissue regeneration. Scaffolds should be able not only to mimic the structure and mechanical functionalities of the tissue during the repair, but also to sense the stimuli emitted by cells and to emit the requited stimuli for cell growth and differentiation [12]. The literature on design of implantable devices that can modulate the release of an active substance in response to external and inner stimuli is abundant [13–15], but *in vivo* demonstration of the capability of the responsive scaffolds to modulate tissue regeneration is still scarce. Moreover, conceiving scaffolds as emitters (not only as transmitters) of stimuli is a recent concept and relies on the hypothesis of that the activation of endogenous signaling pathways may provide more efficient and long-term tissue repair [16,17]. Electrical signals occur continuously at the cell level and are gaining interest as clues for helping the healing process and as alerts of processes that do not occur in the right way. Difficulties in measuring the electrical signals during tissue regeneration made these stimuli to be overlooked in most healing processes (with the exception of nerves), but recent developments in the precise quantification of these signals *in vivo* [18,19] may help unveiling their true potential. The aim of this review is to analyze the state-of-the-art on scaffolds that emit electric signals *in vivo* by highlighting the results already obtained with piezoelectric materials when tested in animal models. First, an overview of the physical properties that can serve as stimuli for the cells during regeneration is provided, with a special focus on piezolectrical signals. Piezoelectric scaffolds for bone, cartilage, tendon and nerve regeneration are presented and the main *in vivo* outcomes discussed in subsequent sections. Wound healing with piezoelectric dressings is tackled in the last section with relevant examples of performance in preclinical studies.

2. Methodology

Information was collected since October 2022 to May 2023 (last update) in the Web of Science Core Collection database (2022, Clarivate). The terms "responsive AND scaffold AND regenerative medicine" rendered 286 outcomes, which were refined by "article" and "*in vivo*" (52 outcomes). A similar search was carried out using the terms "stimulus AND scaffold AND regenerative medicine" and 358 outcomes were obtained. Refinement by "article" and "*in vivo*" rendered 57 outcomes. Replacing "regenerative medicine" in the two former searches by "wound" led to 43 and 20 articles, respectively. Additional searches (refined by "article" and "*in vivo*") were "piezoelectric AND regeneration" with 56 records, and "piezoelectric AND wound healing" with 16 records. As shown in Fig. 1, although the search did not limit the year of

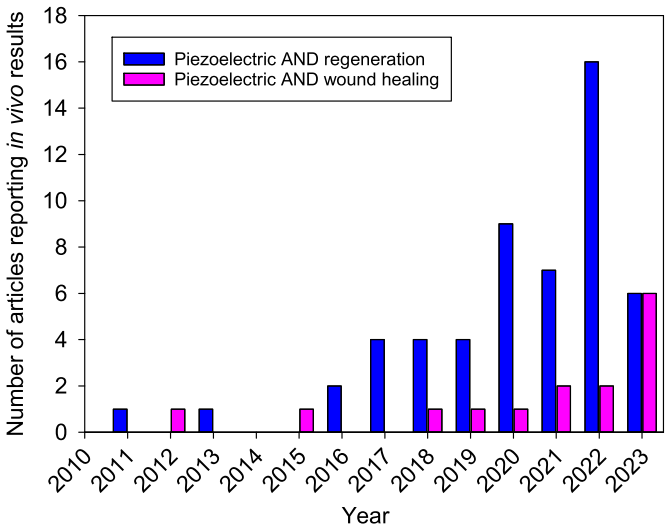

Fig. 1. Records obtained using the Web of Science Core Collection database for the searches shown in the legend after being refined by "article" and "*in vivo*". Results collected on May 6, 2023.

publication, most papers were published in the last decade, showing an increase in the last five years, especially for regeneration with piezoelectric scaffolds. All outcomes were manually screened to identify those dealing with electrical signals and that included tests in animal models. A summary of the original papers that were finally analyzed is provided in Tables 1 and 2. Reviews on these topics were only used to elaborate the context of each section. No clinical trials were found when searching in the ClinicalTrials.gov database.

3. Physical stimuli-emitting scaffolds

The interface between the scaffold and the host cells plays a key role in the success of tissue integration and regeneration. Natural inflammation forms part of the first steps towards healing, but the scaffold should not trigger exacerbated host response that may cause the failure of the treatment [53]. Components from damaged blood vessels may rapidly adsorb on the scaffold surface after implantation. Proteins, lipids, saccharides and ions show different adsorption patterns depending on the surface chemistry, topography and roughness of the scaffold, which in turn determines the subsequent binding of different types of cells [54]. The variety of chemokines and other factors released by immune cells determine the acute and the chronic inflammatory responses against the scaffold. Differently from the classical approaches of designing "immune-evasive" scaffolds that do not elicit immune reactions, there is indeed a need that the scaffolds exhibit immunomodulatory properties facilitating the shift from inflammation to pro-regenerative cascades [55]. "Immune-interactive" scaffolds should ideally attenuate neutrophil activation, balance M1 and M2 macrophage polarization, facilitate Th1 to Th2 lymphocyte switch, and induce the subpopulation of T cells defined as regulatory (Treg) [56]. The immunological profiles (host innate and adaptative immune responses) of a variety of polymers have been revised elsewhere [56].

The pattern itself of the architecture of the scaffold may act as a physical stimulus for cell adhesion and differentiation. The topography of the scaffold may notably determine the conformation of the adsorbed proteins and consequently the adhesion and activation of cells [57]. An adequate design of the topography at both nano- and micro-scales may become a helpful tool for the tuning of direct cell-scaffold interactions [56]. Although most studies have focused on the effects of the topography on modulation of macrophages and other immune cells, there is increasing information on the effects of pore size and shape on other cells that actively participate in tissue regeneration [58].

A step forward in this direction is the precise control of the position of each cell in the scaffold to regulate the cell-cell interactions that occur through diffusible signals and direct contacts. These contacts are important in stem cell differentiation and to form functional tissues [59]. Chips with single-cell resolution have evidenced that colony formation and self-renewal of embryonic stem cells are maximized when each cell is placed in one well separate from other cells [60]. Therefore, the design of niches may have to consider the hosting of single cells while maintaining space in the surroundings to proliferate.

Bioelectrical signals are key stimuli for cells migration and outgrowth as they determine large-scale patterning processes [61]. Natural endogenous unidirectional flow of electric charge has been shown to provide specific instructive signals for tissue formation and remodeling during embryonic development and also after an injury [62]. Bioelectrical signals are key for the morphostasis, that is to say, the maintenance of the target morphology that is acquired during development and should be preserved during cellular turnover along life and after injuries. In human body, the voltage sources are the *trans*-plasma membrane electrical potential and the *trans*-epithelial potential across cells interconnected via strong tight junctions [63]. The electrical potential differences are due to the selective transport of certain ions across the cells (through specific ion channels and pumps situated in the plasma membrane), leading to a net movement of charge (Fig. 2A). The membrane potential normally varies from −40 mV to −90 mV in differentiated cells (inside negative). Low membrane voltages are typical of undifferentiated (e.g., embryonic, stem, or tumor) cells that proliferate rapidly. By contrast, differentiated somatic cells are highly polarized (Fig. 2B) [61,64].

The apical-basal organization of epithelial cells can be assimilated to a parallel arrangement of battery cells with a *trans*-epithelial potential of +50 mV in the epidermis (basal side positive relative to the apical side) and −70 mV in the *trans*-plasma membrane of neurons. These endogenous electric fields behave as steady or slowly changing gradients under healthy conditions. An injury in the plasma membrane or in the tight junctions causes an increase in the electrical current at the site of the injury. Consequently, cells located nearby are subjected to a strong and unidirectional extracellular electric field towards the wound center. In the case of a wound injury the current efflux values are in the 1–10 μA/cm^2 range and the local electric field ranges between 40 and 200 mV/mm and lasts for at least one day. In the case of amputations, the peak of current density may reach up to 100 μA/cm^2 and the field persists for days. Cells and even sheets of cells align, migrate and grow as a function of the direction of the electric field lines, which are tangent to the wound edge (laterally orientated electric field). Bacteria sensitive to electrical fields may also find the best way of get access to the body through the weakest point of an epithelium. Electric fields are important guiding cues for cell migration and may even override biochemical and topographic cues [18].

Most human cells exhibit galvanotaxis and align their long axis perpendicular to the field lines, but they can migrate towards the negative pole (e.g., keratinocytes move towards the center of the wound) or the positive pole. Relevantly, alterations of the membrane voltage trigger a variety of downstream second-messenger cascades in nonexcitable cells that drive transcriptional changes. These changes determine, among others, human mesenchymal stem cell (MSC) differentiation [65] and tumorigenesis [66]. The role of the membrane potential as sensor and actuator against internal and external stimuli is key for critical processes such as cell cycle, proliferation and differentiation, and thus modulation of its value is becoming a relevant therapeutic target for the management of many diseases and biological functions, as recently revised [67,68].

External electrical stimulation has demonstrated to notably accelerate wound healing and tissue regeneration, and indeed it is an approved treatment for chronic wounds since 2002. Various mechanisms are under investigation to explain the beneficial effects of the electrical field in tissue regeneration [63]. However, the introduction of

Table 1
Relevant examples of piezoelectric scaffolds tested *in vivo* for bone regeneration.

#	Piezoelectric component	Scaffold preparation and features	*In vivo* model	Main outcomes	Ref.
1	Poly(vinylidene fluoride) (PVDF)	Electrospun fibers of PU and PVDF (diameter 1.41 μm, pore size 11.47 μm, $d_{33} = 13.96$ pC/N).	Subcutaneous implantation in rats	High fibrosis after 2 weeks of implantation favored by animal movement	20
2	PVDF	Electrospun membranes and poled and non-poled films.	Rats with two defects in femur (3 mm in diameter) separated 1 cm each other. The materials were inserted in the femur and the wound sutured.	Electrospun membranes and poled films promoted bone regeneration after 4 weeks due to the piezoelectricity induced by the animal walking. Non-poled films hindered bone growth.	21
3	Poly(vinylidene fluoride-tri-fluoroethylene) P(VDF-TrFE)	Membranes were annealed (90 °C and 120 °C) to increase the β phase and the d_{33} values (from 10 to 20 pC/N). The were treated with corona poling in a DC field (13 kV, 60 °C, 60 min).	Critical-sized calvarial defects in rats (5 mm in diameter) in each side of the parietal bone, treated with unpolarized, low polarized or highly polarized membranes.	Complete bone defect healing was observed after 8 weeks for rats treated with low polarized membranes.	22
4	P(VDF-TrFE)	Electrospun nanofibers were sputtered with Au electrodes on the top and bottom sides and then poled at 115 °C under an electric field of 100 MV/m for 30 min to induce high piezoelectricity. $d_{31} = 15.73$ pC/N	Subcutaneous implantation in the thigh region of rats.	*In vivo* maximum voltage and current of 6 mV and ~6 nA were recorded. Fibroblasts grew and aligned perfectly along the nanofibers direction.	23
5	P(VDF-TeFE) and hydroxyapatite (HA)	Flexible intramedullary nails (FINs) with or without coating with either P(VDF-TeFE)+HA or calcium phosphate.	Dogs with intervention in fibula and tibia. The dogs were allowed to walk.	Both coatings favored new bone formation, but the area of newborn bone with marrow was greater in the case of P(VDF-TeFE)+HA coating. Compared to the non-coated FIN, those coated with P(VDF-TeFE)+HA increased the relative area of dense bone tissue in the regenerate zone by ca. 39%.	24
6	PVDF	Double layered PVA/PVDF hydrogel with silver nanowires and nano-HA, obtained by freezing—thawing.	Rabbit osteochondral defect model. Three groups: negative control (no scaffold); PVA/HA group; PVA/PVDF/Ag/HA group.	Differently to other treatments, PVA/PVDF/Ag/HA hydrogel integrated in the tissue and facilitated the complete repair of the cartilage and subchondral bone defect in 12 weeks.	25
7	Potassium sodium niobate ($K_{0.5}Na_{0.5}NbO_3$, KNN) nanowires	Electrospun PLA nanofibers with KNN (previously coated with polydopamine) and aligned PLA microstrips prepared by 3D printing. The scaffold was rolled up to form a 2 mm cylindrical device. $d_{33} = 20$ pC/N	Mice spinal cord injury (T9-T11). In absence of animal movement, piezoelectricity was triggered with an external source of ultrasound (US) applied for 20 min every two days from week 0–4.	The US-activation favored neural stem cell differentiation and endogenous angiogenesis in the lesion, and animals showed a better recovery of the motor function.	26
8	PLA	Electrospun PLA nanofibers were annealed (105 °C, 10 h), cooled down, sandwiched between Teflon plated and heated at 160.1 °C for 10 h. Films cut at a 45° angle with the fiber direction.	Calvarial bone defect (3.5 mm diameter) in transgenic mice. Ultrasound treatment started 3 days after the surgery (30 min/day; 5 days a week; 4 weeks).	Highly aligned electrospun fibers responded to US waves with output voltage of 200 mV, and the response was reproducible after 26 days immersed in culture medium.	27
9	PLLA	Aligned (drum speed 4000 rpm) and non-aligned (drum speed 300 rpm) PLLA nanofibers. Annealing at 105 °C for 10 h, cooling down, and second heating at 160.1 °C for 10 h.	Critical osteochondral defects in rabbit model. Animal groups included: (i) piezoelectric PLLA scaffold, (ii) non-piezoelectric scaffold; and (iii) negative control. Two postsurgery conditions were tested: physical exercise or not.	Animals with piezoelectric PLLA scaffold and that follow exercise routine (1–2 months) completely healed the cartilage with abundant chondrocytes. Differently, in the absence of the piezoelectric scaffold the defect was not filled.	28
10	$BaTiO_3$	PLLA:$BaTiO_3$ 80:20 membrane polarized using a corona polarization device. $d_{33} = 4.4$ pC/N 12 weeks after polarization.	Rat cranial defect (5 mm diameter). Treatments included polarized and non-polarized membranes and a negative control (without membrane).	The polarized piezoelectric membrane allowed for a complete recovery of bone in 12 weeks, demonstrating a synergic role between surface charge and piezoelectricity.	29
11	$BaTiO_3$ (Ca/Mn co-doped)	Porous scaffold obtained by blending Ca^{2+}/Mn^{4+} co-doped $BaTiO_3$ nanofibers into the PLLA matrix and freeze-drying. d_{33} ranged from 0.38 pC/N for non-polarized PLLA scaffold to 3.5 pC/N for polarized composite scaffold.	Rat calvarial defect model (5 mm diameter). Polarized (Z-potential −50.45 mV) and non-polarized scaffolds (Z-potential −5.32 mV) were tested for 4 and 8 weeks.	Polarized composites showed improved osteogenic, antibacterial and anti-inflammatory features.	30
12	P(VDF-TrFE) with polydopamine-coated $BaTiO_3$ nanoparticles	Membranes with different contents in $BaTiO_3$ nanoparticles were subjected to corona poling (DC field of 13 kV for 30 min).	Critical-sized calvarial defects in rats (5 mm in diameter) in each side of the parietal bone). Defects on the right were covered with $BaTiO_3$-containing membrane, while the defects on the left were treated with membrane without $BaTiO_3$ or with $BaTiO_3$ or left emptied.	Incipient bone formation at week 4 and complete bone healing at week 12 in those defects covered with $BaTiO_3$-containing membrane. The bone volume and density were higher than for membranes without $BaTiO_3$.	31
13	$BaTiO_3$	Membranes of poly(3-hydroxybutyric acid-co-3-hydrovaleric acid) (PHBV) with $BaTiO_3$ and polydopamine-modified HA.	Critical-sized calvarial defects in rats (5 mm in diameter) treated with: PHBV, PHA, PHA+5% $BaTiO_3$, PHA+10% $BaTiO_3$, or left empty.	Evaluation at week 4 revealed that scaffolds containing $BaTiO_3$ enhanced bone formation not only from the margins of the defect, but also from the center of the defect.	32
14	$BaTiO_3$	3D printed Ti6Al4V scaffold (macropore size 660 μm) coated with $BaTiO_3$ nanoparticles, and subsequent polarization treatment (pTi/	Sheep spinal fusion model to evaluate bony fusion and angiogenesis at 4 and 8 months after implantation.	The piezoelectric scaffold significantly reinforced osteogenesis and angiogenesis.	33

(*continued on next page*)

Table 1 (*continued*)

#	Piezoelectric component	Scaffold preparation and features	*In vivo* model	Main outcomes	Ref.
		$BaTiO_3$ (poled)) or not (pTi/$BaTiO_3$ (unpoled)). d_{33} = 0.7 pC/N			
15	$BaTiO_3$	3D printed Ti6Al4V scaffold (macropore size 660 μm) coated with $BaTiO_3$ nanoparticles (hydrothermal treatment).	Large segmental defect model of the radius in rabbits. Four groups were compared: pure titanium implant (pTi); $BaTiO_3$-coated implant ($BaTiO_3$/pTi); pTi + low-intensity pulsed ultrasound (pTi + LIPUS); and $BaTiO_3$/pTi + LIPUS.	Combination of $BaTiO_3$/pTi + LIPUS significantly enhanced osteogenesis and angiogenesis.	34
16	$BaTiO_3$	Porous Ti6Al4V scaffold coated with $BaTiO_3$ nanoparticles (hydrothermal treatment), followed by corona poling (d_{33} = 0.7 pC/N).	Sheep large segmental bone defects (3 cm) were treated with coated and non-coated scaffolds. LIPUS was applied to some animals immediately after surgery.	The coated scaffold significantly increased the bone volume after 4 months implantation.	35
17	PVDF-TrFE with $CoFe_2O_4$ nanoparticles (CFO/P(VDF-TrFE))	Membranes prepared by the casting method were subjected to alternately positive and negative contact polarization treatments to create microscale straight-stripe distribution of surface potential.	Calvarial defect in rats (5 mm). Two defects were produced per rat, one covered with a negative CFO/P(VDF-TrFE) membrane, and the other with the patterned CFO/P(VDF-TrFE) membrane.	A faster and more uniform bone formation compared was observed with the patterned membranes than the non-patterned ones after 4 and 8 weeks.	36
18	GaN/AlGaN	Ga-polarity GaN/AlGaN films fabricated on SiC substrates (zeta potential of −74.07 mV).	Rat femur defect (5 mm length, 5 mm width, 1.2 mm thickness) with a gap of 0.7 mm in height between the implant surface and the defect bone wall.	Ga-polarity GaN/AlGaN (with a negatively charged surface) nanofilms facilitated attachment, spreading, recruitment, and osteogenic differentiation of MSCs and promoted bone repair *in vivo*.	37
19	$K_{0.5}Na_{0.5}NbO_3$ (KNN)	The ceramic was laser-irradiated to mimic the parallel interspersed domains of high/low piezoelectricity of bone ECM (laser-irradiated KNN).	Rabbit formal condyle bone defect model (5 mm long and 3 mm wide). Defects were produced in the knee joint parallel to the long axis of the femur. The ceramic was placed with the positively polarized side faced the deep side of bone marrow cavity.	Greater bone regeneration and new bone was firmly attached to the laser-irradiated KNN ceramic, compared to pristine KNN.	38

electrodes to mimic the natural stimulus for electrotherapy is not feasible, or at least very hardly achievable, in internal tissues. The risk of infections is also a drawback. Alternatively, electrical stimulation may be accomplished by either developing conductive scaffolds that can be externally stimulated using non-invasive devices [69,70] or designing piezoelectric scaffolds that generate themselves the electric fields when become deformed (pressure-induced electricity) [71,72].

A variety of tissue cells in our body express PIEZO1 and PIEZO2 mechanosensitive cation channels. PIEZO1 and PIEZO2 are transmembrane proteins that become activated by membrane stretch. The performance of PIEZO channels, in health and in disease, determines key physiological process at molecular, cellular and system level [73]. PIEZO1 functions are mainly in non-sensory tissues that are subjected to mechanical stress, fluid pressure or shear, and are involved in maintaining muscle and bone mass, sensing tendon stretch, and regulation of senescence and apoptosis in response to mechanical as well as electrical stimuli. PIEZO2 are abundant in sensory tissues and participate in the transduction of pain and touch sensations as well as proprioception in the nervous system. The last decade advances evidenced that PIEZO channels are critical for the health of musculoskeletal system, and the modulation of their performance may open novel avenues for therapy and regeneration [74].

Piezoelectricity is defined as the electric polarization in a substance in response to the application of mechanical stress. The linear conversion of mechanical energy to electrical energies, which is given by Equation (1), is a property typical of non-symmetric substances [75].

$$\{D\} = [d]\{T\} + [\varepsilon^t]\{E\} \quad (1)$$

In this Equation, D represents the electrical displacement, [d] the direct piezoelectric effect matrix, T is a constant stress field, [ε^t] the transpose of the permittivity matrix, and E the electrical field strength.

The inverse conversion of electrical to mechanical energy is given by Equation 2

$$\{S\} = [s^E]\{T\} + [d^t]\{E\} \quad (2)$$

Where S represents the strain, [s^E] the compliance in a constant electrical field, and [d^t] the matrix for the inverse piezoelectric effect.

A stress applied on a substance that lacks a center of symmetry generates dipole moments that create a net polarization on its surface. This is the case of most biological macromolecules such as DNA, collagen and non-collagen proteins.

Piezoelectric scaffolds perform as stimulus-emitting devices and are particularly useful for nerve tissue repair, bone regeneration and wound healing [76,77]. Piezoelectric biomaterials transform mechanical energy into electric polarization without the need of external power sources (battery-less) [72]. A small deformation of a piezoelectric material due to elongation, twisting, bending or compression causes an imbalance in the ions and charges (charges redistribution), which induces a net dipole moment greater than zero. The mechanically-induced transient surface charge has been shown to induce proliferation and differentiation of stem cells. Polarization of biomaterials can also be produced by forcing the unidirectional orientation of randomly distributed dipoles via a poling process, commonly applying high voltage (1–10 kV).

4. Piezolectric scaffolds for bone and cartilage regeneration

Bone itself is a piezoelectric tissue (0.7–8.7 pC/N) mostly due to the packed aligned collagen fibrils and, to a lesser extent, to the hydroxyapatite crystals [78–80]. The extracellular matrix (ECM) of bone can be represented as parallel domains of piezoelectric collagenous materials and nonpiezoelectric noncollagenous materials, which in turn causes a spatial distribution of positive charges in the collagenous domains. Other collagenous tissues also exhibit piezoelectricity as well as a variety of ordered natural polymers such as polysaccharides and polynucleotides. In addition to piezoelectricity, the *in vivo* load (stress) causes a streaming potential due to the flow of the ions of the interstitial fluid through the bone [81]. Calcium (Ca^{2+}) and phosphate (PO_4^{3-}) ions can be attracted to the electrical dipole, contributing to the growth of the bone, to the effective integration of the implant material in the host bone, and to the development of callus in living bone [82,83].

Piezoelectric response of the intervertebral discs has recently been measured [75]. The intervertebral disc is formed by a nucleus pulposus (NP, a gel-like type II collagen and proteoglycans dispersion) wrapped by the annulus fibrosus (AF, rich in type I collagen) and the cartilaginous

Table 2
Relevant examples of piezoelectric scaffolds tested *in vivo* for regenerative medicine purposes in tissues other than bone.

#	Piezoelectric component	Scaffold preparation and features	*In vivo* model	Main outcomes	Ref.
1	Poly(vinylidene fluoride-co-trifluoroethylene), P(VDF-TrFE)	Aligned electrospun nanofibers of P(VDF-TrFE) (390–550 nm) collected on a disk at a short distance and rotating at high speed (d_{33} = 36.5 pC/N) The nanofibers were grafted with poly (acrylic acid) and then coated with fibronectin. Non-piezoelectric PTFE scaffold was used as a control.	Full-thickness Rat Achilles acute tendon injury model (5 mm of tendon was removed). Tendon were sutured end to end while placing P(VDF-TrFE) or PTFE scaffold in the defect or maintaining the defect without scaffold. 2 weeks after injury, the animals were divided into two groups: one with a treadmill running (MTR) protocol, and one that remained in the cage (Cage).	8-week post-injury, animals that follow MTR protocol increased their functional recovery compared to Cage animals. Collagen I/III synthesis and tendon specific proteins were significantly increased in animals treated with P(VDF-TrFE) and MTR. Differently, in the absence of the piezoelectric scaffold BMP expression was increased.	16
2	Boron nitride nanosheets	PCL composite scaffold obtained through 3D layer-by-layer droplet spraying method.	Rat model with 15 mm sciatic nerve cut. Treadmill running was considered for one group of animals.	Piezoelectric scaffolds restored bioelectrical signal conduction and attenuated the immune response. The distal nerve end was recovered through enhanced microvessels, and finally muscle reinnervation was possible.	39
2	ZnO	Aligned electrospun nanofibers of PCL and ZnO that were rolled into nerve conduits.	Unilateral sciatic nerve defects of 10 mm in rat model. Three groups of animals: (a) treated with PCL-ZnO mats, (b) treated with PCL mats; and (c) in situ reconnection of the cut nerve (terminal–terminal bridging).	Animals treated with PCL-ZnO mats showed faster morphological and functional recovery, with enhanced NGF, VEGF and S100 (a marker of Schwann cells) levels.	40
3	ZnO	3D injectable multilayer molding technique to obtain porous PCL scaffold with ZnO nanoparticles (30–80 nm).	A 1.5 cm sciatic nerve gap in a murine model. Three groups treatment: the ZnO/PCL scaffold group, PCL scaffold group, and autograft group (original nerve group reversed by 180°). After implantation, rats start physical exercise (treadmill training 30 min/day).	Running practice improved the recovery in all rats, but more in those wearing the piezoelectric scaffolds. The sciatic function index and the muscle fiber density and weight were significantly higher in animals treated with the piezoelectric scaffold.	28
4	PVDF-TrFE	Electrospun scaffolds with aligned or randomly oriented fibers were rolled into a hollow conduit (5 mm length) with an inner diameter of 2.4–2.7 mm and outer diameter of 2.5–2.8 mm.	The spinal cord of female adult rats was completely transected at T8, and a gap of 2.5 mm was created. The rostral stump was inserted into the conduit and then the caudal stump into the other end. A GFP-SCs/matrigel mixture was introduced in the conduit.	3 weeks post-transplantation the GFP-SCs were uniformly distributed along the aligned conduits. Close association of GFP-SCs with NF + axons also occurred.	41
5	PVDF/ZnO	Electrospun mats were sandwiched in PDMS and connected to conduits prepared with conductive materials (chitosan, PEDOT and PLLA).	SD rats with the PVDF/ZnO device implanted in the thorax subcutaneous adipose tissue, and the conductive conduit in a 15 mm defect of the sciatic nerve. Both devices were connected by polypropylene encapsulated soft Pt wire.	Compared to the autograft group (original nerve group reversed by 180°), the devices provided similar growth of newborn Schwann cells and myelin-rich nerve fibers.	42
6	Carbon nitride C_3N_5 nanosheets	Microneedles made of platinum–ruthenium nanoalloys and carbon nitride C_3N_5 nanosheets.	Methicillin-resistant *Staphylococcus aureus* (MRSA)-infected mouse wound model. Mice were treated with microneedles made with nanoalloys and nanosheets in separate or mixed together. Some animals received US treatment.	Combination of the piezoelectric needles and US treatment eradicated the bacterial colonies after 9 days of treatment.	43
7	Au@$BaTiO_3$	$BaTiO_3$ nanocubes with gold nanoparticles reduced on the surface.	Female mice with *S. aureus*-infected full-thickness skin wound were treated with Au@$BaTiO_3$ with and without US activation. Control groups included no treatment and US treatment.	Au@$BaTiO_3$ with US activation provided the fastest healing on day 13, with the tissue showing continuous epidermal layers with follicles and few inflammatory cells, and no bacteria. Differently, the other three mice groups had bacteria in the growing epidermis.	44
8	ZIF-8@$BaTiO_3$	$BaTiO_3$ nanoparticles coated with ZIF-8 loaded with ciprofloxacin.	Male mice with *S. aureus*-infected full-thickness skin wound were treated with bare, ZIF-8 and ZIF-8+drug coated $BaTiO_3$, with or without application of US.	US irradiation was revealed as critical to produce ROS species and to accelerate ciprofloxacin release from the piezoelectric material, and to promote cell migration and wound healing.	45
9	$MoSe_2$	Nanoflowers were prepared according to a one-pot hydrothermal process.	Male mice with *S. aureus*-infected full-thickness skin wound were treated (1 day after) with $MoSe_2$ suspension for 15 min and optionally US (5 min).	Mice treated for 3 days with $MoSe_2$ and US showed at day 7 a lesion reduction of 90%, compared to 20% in the absence of US.	46
10	PLLA with vitamin B2	Films annealed for 1 h at 140 °C.	Male rats with skin wounds treated with US, US + PLLA, or US + PLLA + vitamin B2 for 14 days. US was applied 30 min/day.	Lesions treated with US + PLLA + vitamin B2 showed higher collagen deposition and vascularization on days 7 and 14.	47
11	Polydioxanone (PDX)/poly (hydroxybutyrate-co-valerate) (PHBV) 20/80	Electrospun core–shell PDX/PHBV mats.	Full thickness wound (6 mm in diameter) in rats.	The PDX/PHBV mats decreased fibrosis and accelerated scarless wound regeneration compared to non-treated controls and PDX solely mats.	48

(*continued on next page*)

Table 2 (*continued*)

#	Piezoelectric component	Scaffold preparation and features	*In vivo* model	Main outcomes	Ref.
12	Poly(vinylidene fluoride-tetrafluoroethylene), P(VDF-TeFE)	Electrospun nanofibers of 0.8 μm diameter. Some mats were coated with Cu using magnetron discharge plasma.	Oral mucosa lesion (7 × 4 mm) in rats. Three groups: negative control (without bandages), pristine VDF-TeFE membrane, and VDF-TeFE membrane treated with Cu.	After 3 days of treatment, control wounds were infected and showed edema and necrosis. Oppositely, the two other groups had lower area lesions, showing more granulation tissue and newly formed vessels. After 7 days, the lesions of the mats-treated animals were much smaller with abundant connective tissue.	49
13	P(VDF-TrFE) with tetrabutylammonium chloride (TBAC)	Electrospun mats of P(VDF-TrFE)/TBAC were more crystalline and showed higher output voltage than those of P(VDF-TrFE).	Rats with incisions (3 cm in length) on both sides of the spinal column. One side was used as non-treated control, whereas the other side was sutured with the piezoelectric membrane.	After 7 days treatment, the wound healing was 100% for P(VDF-TrFE)/TBAC and 70% for P(VDF-TrFE). Hair follicles were recovered in the P(VDF-TrFE)/TBAC group.	50
14	P(VDF-TrFE) with TBAC and Fe_3O_4	Wound dressing with one layer of piezoelectric electrospun nanofibers on top of a bioadhesive conductive hydrogel.	Large full-thickness wounds (SD rats; 10 × 20 mm) on both sides of dorsum. One wound was treated with the hydrogel solely, while the other wound was treated with the two-layers dressing.	The two-layers dressing provided a wound closure of 80% in the first week (vs. 53% for the hydrogel) and notably enhanced the expression of bFGF, PDGF, and VEGF.	51
15	Chitosan	Chitosan film with different contents in polydopamine exhibited piezoelectric and photothermal properties.	Full-thickness wounds in male rats, which were covered with chitosan or chitosan/polydopamine films and irradiated or not with NIR laser (9 min on day 0, 4 and 7).	Piezoelectricity was enhanced by polydopamine and NIR irradiation, which resulted in up-regulation of heat shock protein 90 and hypoxia-inducible factor 1 α. This treatment showed the fastest wound healing.	52

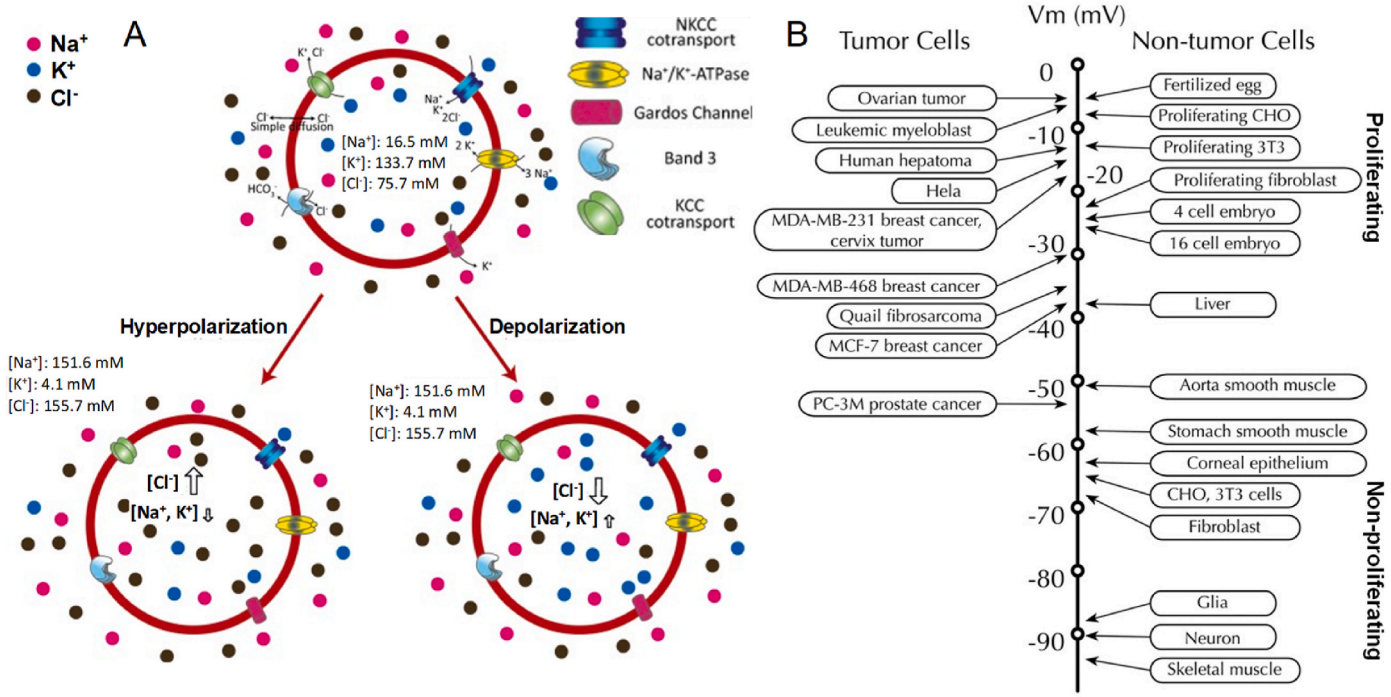

Fig. 2. (A) Plasma membrane potential in cells (e.g., erythrocytes) is orchestrated by ion permeability (mainly Cl^-) and specific transporters (e.g., for K^+ and Na^+). Hyperpolarization involves an increase in intracellular negative charges, while depolarization is shown as a decrease in the absolute values of plasma membrane potential. Reproduced from Balach et al. [19] with permission from Springer Nature. (B) Membrane potential (Vm) of a variety of cells, with values close to zero corresponding to rapidly proliferating cells and the most negative values to quiescent cells. Reproduced from Yang and Brackenbury [64] under Creative Commons Attribution License.

endplates (between the vertebral endplate and the nucleus pulposus). Using Piezoresponse Force Microscopy (PFM), AF showed stronger piezoelectricity according to its collagenous nature, but NP study revealed that non-collagenous proteins also contribute to the piezoelectric properties. *In vivo*, the longitudinal stress was shown to cause a local piezoelectricity of 2 mVm/N, which directly determines cell alignment in AF.

Electrospinning has been shown as a suitable technique to obtain piezoelectric scaffolds. The nanofibers may be sensitive to the cell traction force; namely after cell adhesion, the intracellular tension that is generated in the cell when intends to spread is transmitted to the substrate and then a counterforce is generated. The distortion of the nanofibers may trigger their electrical signal in accordance with the strain level, usually in the range of few nanoNewtons [84]. Greater scaffold strain can be induced by the movements associated to physiological movements and daily activities (breathing, heart beating, walking) and also by using an external source of energy, such as ultrasonic irradiation. The most promising piezoelectric polymers are

polyvinylidene fluoride (PVDF; $d_{33} = -25$ pC/N) and poly-L-lactic acid (PLLA; $d_{14} = -9.82$ pC/N); polarization in these polymers can be achieved through compression/stretching and shear, respectively [76]. Subcutaneous implantation of electrospun dressings of polyurethane (PU) and PVDF (as β phase) in animal vertex, abdomen and back evidenced strong growth of fibroblasts due to the animal movements, compared to the non-piezoelectric PU scaffolds (Table 1, entry #1) [20]. Similarly, subcutaneous implantation of PU sponges coated with PVDF and calcium phosphate were shown to induce ectopic bone formation [85].

Poled PVDF films ($d_{33} = -24$ pC/N) and electrospun fibers ($d_{33} = -48$ pC/N) have also demonstrated piezoelectric features suitable for bone regeneration [21]. *In vivo* studies carried out in critical defects in femur revealed that non-poled films did not aid bone regeneration. Differently, poled films and electrospun fibers promoted bone marrow and trabecular bone formation. Compared to poled films, the electrospun fibers allowed cell colonization and tissue growth through the fibers, although also favored inflammatory response. (Table 1, entry #2).

Annealing treatment (heating in the 90–140 °C range) can be exploited to tune the content in β phase and, in turn, the surface potential and the piezoelectric coefficients of poly(vinylidene fluoride-trifluoroethylene), P(VDF-TrFE), membranes [22]. Corona poling treatment makes that the electric dipoles reorient in the direction of poling electric field and, as a consequence, induced charges appear on the surface of the material. When the material covers the bone defect, the bone marrow mesenchymal stem cells (MSCs) are attracted by galvanotaxis and differentiated into osteoblasts. Interestingly, membranes with intermediate d_{33} (10 pC/N) and surface potential (−53 mV) have shown better osteogenic properties *in vivo* than unpolarized mats and highly polarized mats ($d_{33} = 20$ pC/N; −78 mV). The P(VDF-TrFE) membranes with intermediate piezoelectric performance enhanced MSC differentiation to bone and caused less production of reactive oxygen species (ROS) by the mitochondria. These membranes performed as efficient periosteum substitutes for calvarial bone reconstruction (Table 1, entry #3). The electrospinning conditions (solution concentration, collector distance, …) have also been shown to strongly determine the piezoelectricity of P(VDF-TrFE) nanofibers [23]. The nanofibers were sputtered with Au electrodes on the top and bottom sides and then poled at 115 °C under an electric field of 100 MV/m for 30 min to induce high piezoelectricity. Then, the nanofibers were encapsulated in poly(dimethylsiloxane) and implanted subcutaneously under the skin of the leg (rat model) (Table 1, entry #4). The leg was pulled using a linear motor system at 0.5 N and 1 Hz frequency (mimicking daily activity) and the scaffold generated an output voltage of 6 mV and output current of 6 nA [23].

Poly(vinylidene fluoride-tetrafluoroethylene), P(VDF-TeFE), combined with hydroxyapatite (HA) has been tested for the coating of flexible intramedullary nails (FINs) that are commonly used to lengthen long tubular bones [24]. FINs of three types were tested: non-coated stainless-steel, calcium phosphate-coated titanium, and P(VDF-TeFE)+HA-coated stainless-steel. Both coatings favored cell adhesion and stimulated *in vitro* the differentiation of MSCs into osteoblasts, as evidenced in the ectopic osteogenesis tests. Moreover, the higher formation of new bone in a dog model observed for the P(VDF-TeFE)+HA-coated FIN was attributed to their piezoelectric properties, but no information on these features was provided (Table 1, entry #5).

In a recent study, a double-layer piezoelectric PVDF hydrogel was prepared by combination with polyvinyl alcohol (PVA) for the repair of osteochondral defects [25]. Articular cartilage is one of the most challenging tissues to be repaired because it is avascular, it has few cells, and the metabolic activity of mature chondrocytes is low. Despite cartilage is a piezoelectric tissue, piezoelectricity has barely been investigated for its repair [86]. In the double-layer PVA:PVDF 15:15 hydrogel, silver nanowires (0.3% final concentration) were used to promote the formation of PVDF β phase and also to prevent from infections in the layer to be in contact with cartilage (chondrogenic layer). The layer to be in contact with bone (osteogenic layer) contained nano-hydroxyapatite (Table 1, entry #6). *In vivo* studies carried out in a rabbit osteochondral defect model involved three groups of treatments for 12 weeks: blank (no scaffold), PVA/HA hydrogel, and PVA/PVDF/Ag/HA hydrogel (Fig. 3). Compared to the blank (no repair) and PVA/HA hydrogel (small amount of cartilaginous tissue), the most piezoelectric PVA/PVDF/Ag/HA hydrogel was perfectly integrated in the tissue and facilitated the formation of cartilage and bone. Relevantly, piezoelectricity had positive effects on osteochondral tissue regeneration and simultaneously facilitated the *in vivo* degradation of the scaffold [25].

Although the piezoelectric performance of PLLA has been less investigated, it has been shown that highly oriented PLLA chains (obtained by mechanical stretching) may endow rods with piezoelectric features useful to enhance bone regeneration *in vivo*, notably enhancing the external callus volume [87]. Improvement of PLLA piezoelectric features requires a careful maximization of both orientation and crystallinity [88]. Similarly, silk fibroin films showed enhanced piezoelectricity by increasing orientation and crystallinity [89]. Interestingly, electrospun PLLA mats can be prepared mimicking the gradual changes in piezoelectricity typical of the cartilage (less piezoelectric)-bone (more piezoelectric) interface. To do that, aligned nanofibers were polarized in a DC electric field at different distances (from 1 to 13.3 cm) for 20 min to regulate the piezoelectricity (Fig. 4). The β phase increased from 33% to 91% as the electric field increased from 1.5 to 20 kV/cm. The adhesion and growth of MSCs on the electrospun mats caused tensions that triggered the piezoelectric signals, which in turn stimulated the selective differentiation of the cells to chondrocytes in the less piezoelectric region and to osteoblasts in the most piezoelectric region [90]. The feasibility of obtaining osteochondral repair remains to be elucidated *in vivo*.

Relevantly, when the lesion compromises the movement of the affected tissue or the patient, remote mechanical activation by means of ultrasound may allow a fine control of the duration and intensity of the electrical stimulation. The feasibility of this approach has recently been demonstrated for PLLA nanofibers loaded with piezoelectric potassium sodium niobate ($K_{0.5}Na_{0.5}NbO_3$) nanowires and used to repair spinal cord injuries (Table 1, entry #7) [26]. Highly aligned PLLA nanofibers solely can also be activated *in vivo* using externally applied ultrasound (Table 1, entry #8). Interestingly, the piezoelectric response was reproducible after 26 days immersed in culture medium, and the stem cell cultures showed significantly higher expressions of alkaline phosphatase (ALP), mineral formation, and osteogenic genes, compared to non-applied ultrasound conditions. The expressions of bone sialoprotein (BSP, green) and dentin matrix protein (DMP, red) were higher for nanofibers subjected to ultrasounds (Fig. 5). *In vivo* studies in calvaria bone of mice confirmed that the animals with implanted piezoelectric PLLA nanofiber films and ultrasound treatment had more new-bone formation than the other groups [27].

PLLA based nanofibers have been tested for the healing of knee joint as a piezoelectric scaffold that can generate electrical stimulation under the joint's motion (Table 1, entry #9). Electrospinning using a drum speed of 4000 rpm rendered piezoelectric fibers, compared to the non-piezoelectric fibers obtained with the same composition on a drum at 300 rpm. The scaffold was prepared with three layers of PLLA nanofiber mat (the second one oriented at 90° with respect to the first and the third ones) and alternating layers of collagen, and then freeze-dried. *In vitro* studies demonstrated that the piezoelectric stimulation significantly enhanced the adsorption of proteins on the scaffold, promoted cell adhesion and triggered calcium ion influx, which in turn favored the secretion of TGF-β1. *In vivo* tests in critical-size cartilage defects in a rabbit knee model evidenced the higher healing capacity (more chondrocytes, collagen, and mechanical resistance) in animals treated with the piezoelectric scaffold and that did physical exercise (1 month rest after the surgery, followed by 20 min treadmill/day for 2 months). Even in the absence of a specific physical training, the piezoelectric scaffolds led to better recovery of the cartilage compared to the non-piezoelectric

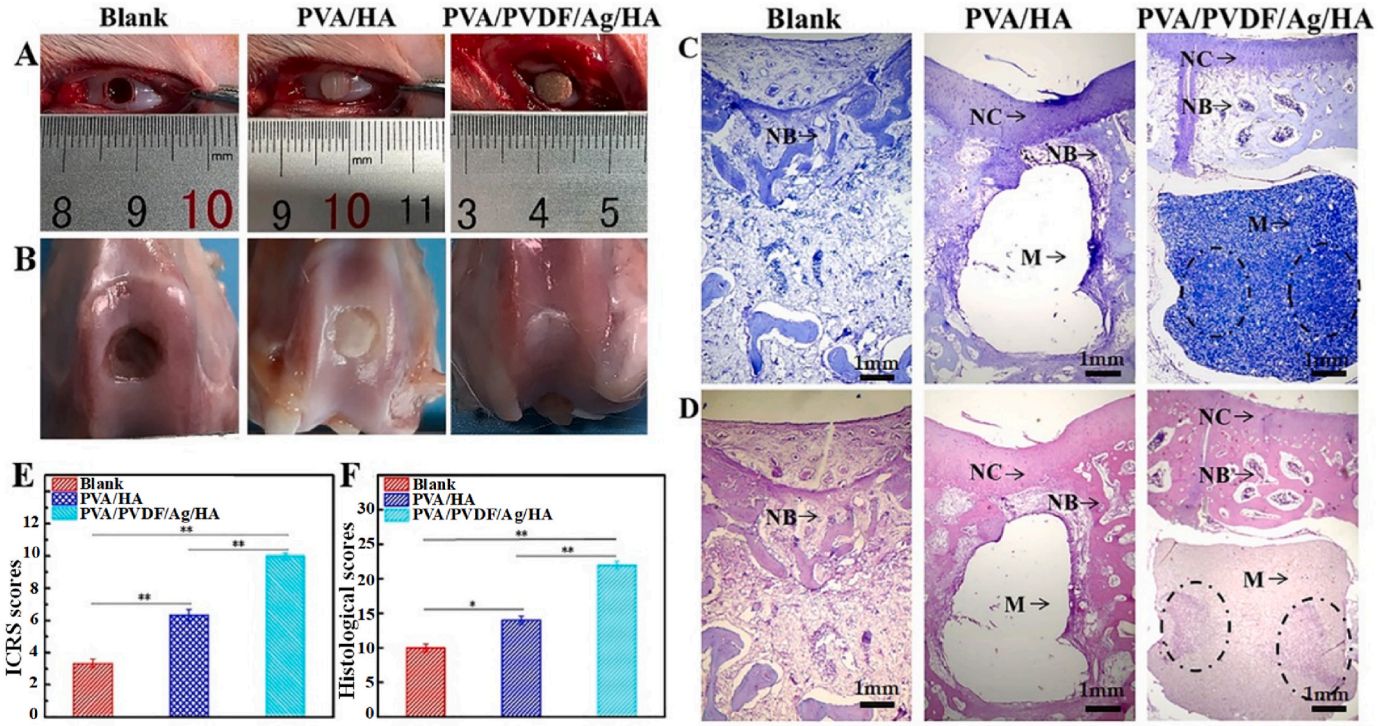

Fig. 3. (A) Full thickness osteochondral defects (diameter 5 mm) on the trochlear groove using a surgical drill (right knee of female rabbits). (B) Images of knees after 12 weeks treatment. (C) Toluidine blue staining of the knees after 12 weeks. (D) Hematoxylin and eosin staining of the knees after 12 weeks. (E) Scores of blank group, PVA/HA group, and PVA/PVDF/Ag/HA group at 12 weeks post-surgery following International Cartilage Repair Society criteria. (F) Histological scoring for evaluating osteochondral defects (*p < 0.05, **p < 0.01). NC: new cartilage; NB: new bone; M: scaffold materials. The area marked with circles showed the ingrowth of new bone. Reproduced from Wu et al. [25] under Creative Commons Attribution (CC BY) license.

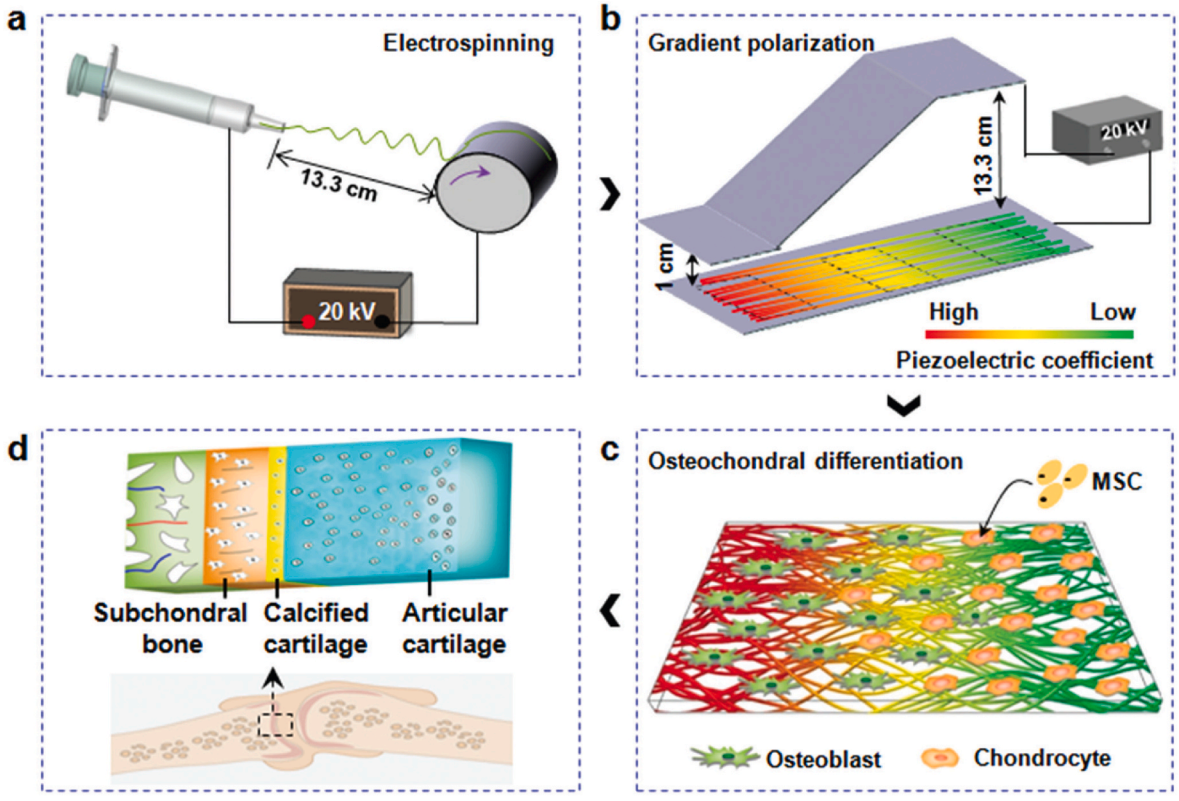

Fig. 4. (a) Electrospinning conditions of PLLA; (b) gradient polarization of PLLA electrospun mat to generate a piezoelectricity gradient; (c) MSCs growing on the mat differentiated *in vitro* to chondrocytes in the less piezoelectric region and to osteoblasts in the most piezoelectric region; (d) the developed tissue resembled the structure of cartilage-bone interface. Reproduced from Liu et al. [90] with permission of the Royal Society of Chemistry.

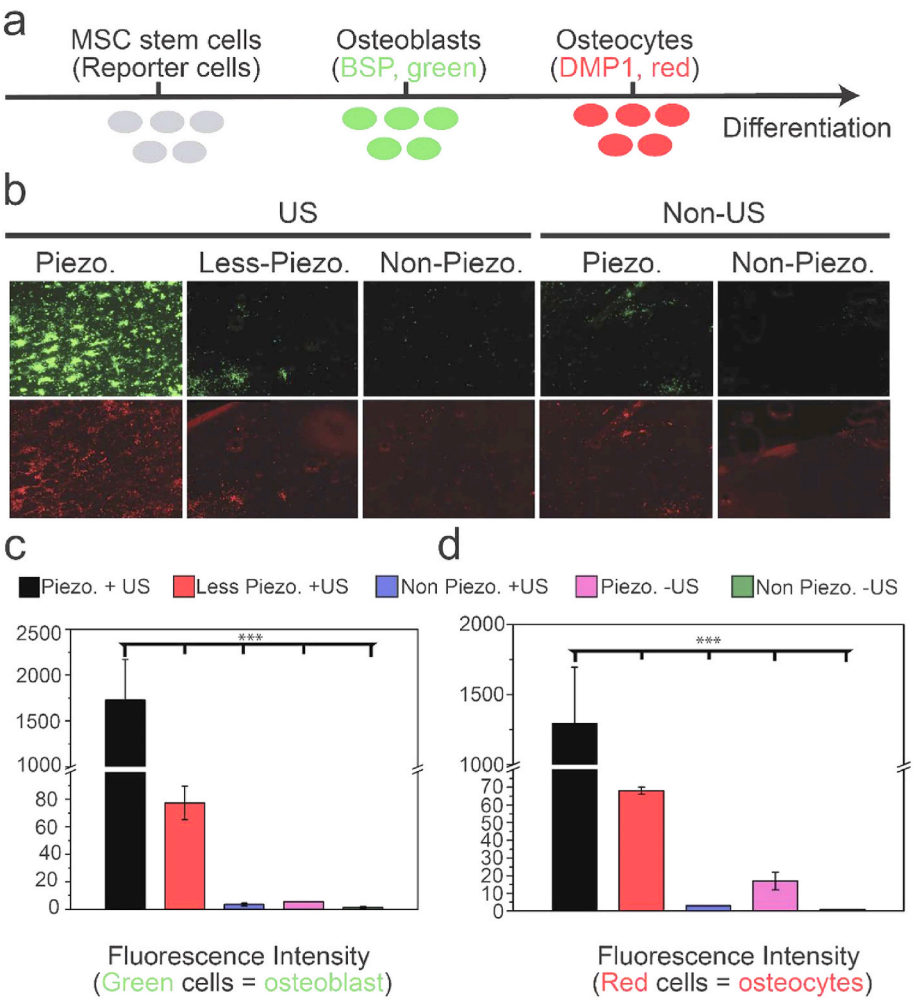

Fig. 5. Osteogenic activity of bone marrow stem cells (BMSCs) cultured on the electrospun PLLA scaffolds with and without ultrasound (US) treatment. The nanofibers were obtained using a collector spin speed of 300 rpm, 1000 rpm, and 3000 rpm and were coded as non-piezoelectric, less piezoelectric and piezoelectric, respectively. (a) Scheme of the change in fluorescence during progressive expression from BSP to DMP. (b) Fluorescent microscope images of the cells seeded on scaffolds subjected to different treatments as observed under the GFP channel and cherry red channel. (c, d) Fluorescent intensity recorded for osteoblasts and osteocytes. Two tailed *t*-test for statistical analysis: ***p = 0.0001. Reproduced from Das et al. [27] with permission of Elsevier.

scaffolds probably because the natural movement of the rabbit activated the scaffold [28].

Additives such ZnO, (Na,K)NbO_3, carboxylated multiwalled carbon nanotubes, exfoliated boron nitride nanosheets, and barium titanate ($BaTiO_3$) have been shown useful to endow biodegradable scaffolds with piezoelectric properties for bone regeneration and nerve repair [71,91,92]. $BaTiO_3$ is a commonly tested biocompatible lead-free ceramic for bone repair exhibiting piezoelectric features. Porous composites (ice templated) of HA and $BaTiO_3$ in the mass ratios of 30/70 and 10/90 had piezoelectric coefficient d_{33} of 1.2 and 2.8 pC/N, which is above that of the bone itself (0.7 pC/N) [93]. PLLA membranes containing $BaTiO_3$ were obtained using a solution casting method followed by corona polarization treatment (4.4 pC/N). *In vivo* studies were carried out in rat cranial defects comparing polarized and non-polarized membranes and also a control without membrane. Polarized piezoelectric membranes allowed for a complete healing in 12 weeks, with mature osteoblasts and bone (Table 1, entry #10). Differently, the other treatments only showed a small amount of new bone at the margins [29]. Ca/Mn co-doped $BaTiO_3$ (CMBT) nanofibers were prepared to facilitate the mixing with aligned PLLA chains and to promote bone formation through the sustained release of Ca^{2+} and Mn^{4+} ions (Fig. 6) [30]. Pre-treatment of PLLA and PLLA/CMBT scaffolds (freeze-dried sponges) with a DC electric field of 6 kV/cm at room temperature for 30 min for polarization was shown to notably improve bone volume to total volume fraction (BV/TV) and bone mineral density in rat calvarial defects (Table 1, entry #11). Therefore, the surface charges of the scaffolds were evidenced to play a role in the regeneration of bones with low stress loads.

P(VDF-TrFE) membranes have also been shown to benefit from the incorporation of $BaTiO_3$ nanoparticles. As an example, membranes containing polydopamine-coated $BaTiO_3$ nanoparticles (5 vol%) that were subjected to corona poling treatment maintained a strongly negative surface potential (−76.8 mV to −40 mV range) for more than 12 weeks in the bone defect conditions (Table 1, entry #12) [31]. Polydopamine can be considered as a multifunctional material that improves the compatibility among different materials (the main purpose in this example), can be versatile modified with a variety of functional groups and substances, and also exhibits photothermal capabilities [94]. *In vivo* studies in rat calvarial models evidenced the capability of the hybrid membranes to induce a rapid recovery of the bone through higher increase in the number of cells and also in ALP activity and mineral deposition compared to membranes without nanoparticles. Interestingly, the membranes did not adhere to the growing bone which may allow easy removal of the membranes after bone healing, if needed [31].

A spin-coating method has recently been implemented to mimic the periosteum by means of a poly(3-hydroxybutyric acid-co-3-hydrovaleric acid) (PHBV) scaffold containing $BaTiO_3$ and HA modified with polydopamine to improve materials compatibility and also to favor cell adhesion. The obtained membrane exhibited immunomodulatory capability by suppressing ROS species and inducing M2 macrophage polarization, and also strong osteogenic activity in a critical-sized cranial defect in rats (Table 1, entry #13). Relevantly, the hybrid membrane combining the three components induced bone formation from the defect edges and also from inside the defect area as it enabled intramembranous ossification and vascularization [32].

$BaTiO_3$ has also been combined with porous metallic scaffolds. For

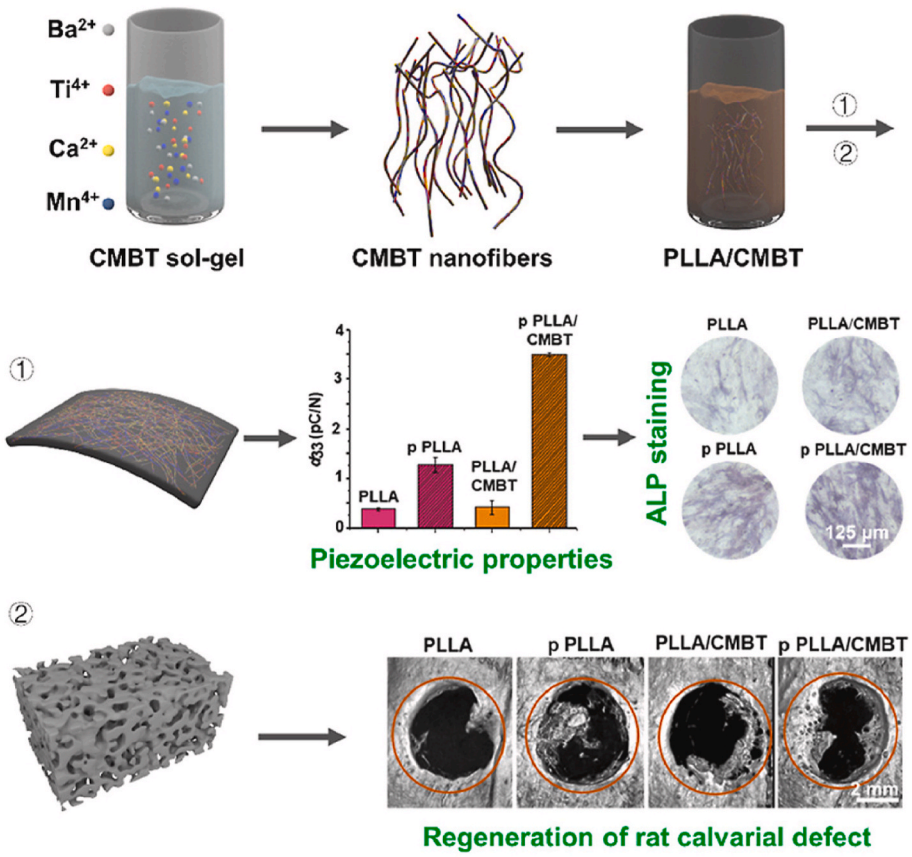

Fig. 6. Ca/Mn co-doped $BaTiO_3$ (CMBT) nanofibers were prepared by electrospinning and subsequent calcination. Then, the nanofibers were used to prepare (1) PLLA composite membranes via solution casting, which were polarized (p) or not and used for *in vitro* monitoring of stem cells differentiation, and (2) porous PLLA sponges via freeze-drying. In a rat calvarial model, polarized sponges (p PLLA and p PLLA/CMBT) notably promoted bone regeneration compared to non-polarized counterparts (PLLA and PLLA/CMBT). Reproduced from Zheng et al. [30] with permission of Elsevier.

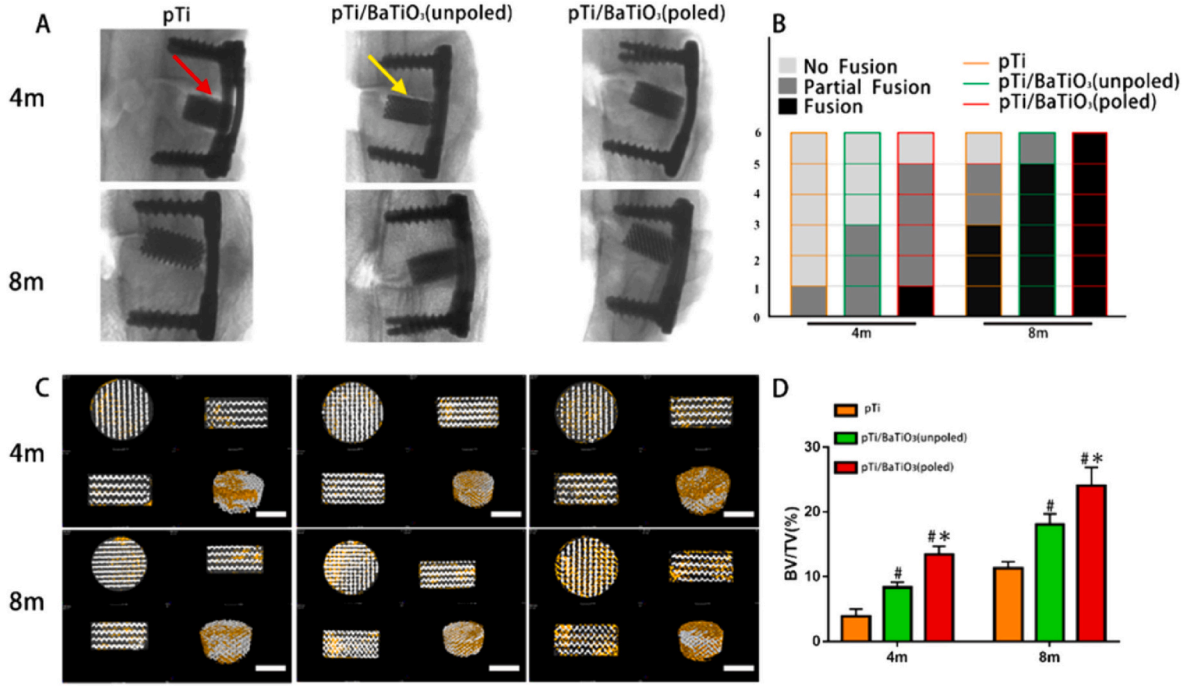

Fig. 7. Results obtained after *in vivo* implantation (intervertebral fusion surgery) of porous Ti6Al4V cylinders (12 mm diameter and 6 mm height). The scaffolds were used as non-coated (pTi) and after being coated with $BaTiO_3$ ceramic without and with polarization treatment (pTi/BaTiO3 (unpoled) and pTi/BaTiO3 (poled), respectively). (A) Radiographs after 4 and 8 months postoperation, showing no fusion (red arrow) and partial fusion (yellow arrow). (B) Radiologic evaluation of spinal fusion. (C) 3D micro-CT images (scale bar = 6 mm) used to detect bone ingrowth and angiogenesis. (D) Quantitative analysis of micro-CT reconstructions in terms of percentage of bone volume/total volume (BV/TV) in the region of interest chosen to evaluate bone ingrowth ability. #$p < 0.05$ vs the pTi group; *$p < 0.05$ vs the pTi/BaTiO3 (unpoled) group. Reprinted from Liu et al. [33] with permission of the American Chemical Society. Copyright © 2020 American Chemical Society.

instance, porous metallic scaffolds of Ti6Al4V (600 μm pore size; 70–90% porosity) coated with $BaTiO_3$ evidenced their capability to reinforce osteogenesis and angiogenesis compared to non-piezoelectric controls in a sheep spinal fusion model [33]. Three types of scaffolds were tested: non-coated ones (pTi), coated with $BaTiO_3$ piezoelectric ceramic without polarization treatment (pTi/BaTiO3 (unpoled)), and coated followed by polarization treatment (pTi/BaTiO3 (poled)) (Table 1, entry #14). X-ray and micro-CT images revealed that the pTi/BaTiO3 (poled) group notably accelerated the fusion with higher percentages of bone volume/total volume (BV/TV) inside the scaffold (Fig. 7). Posterior studies have shown that the performance of low piezoelectric $BaTiO_3$-coated scaffold can be improved by external application of low intensity pulsed ultrasound (LIPUS) (Table 1, entry #15). Enhanced osteogenesis and osseointegration was recorded at 6 and 12 weeks after implantation of pTi/BaTiO3 in the radius of rabbits and application of LIPUS for 20 min daily for 6–12 weeks [34]. The combination of piezoelectricity and LIPUS has also been shown useful to aid porous titanium scaffolds in restoring the physiological environment in large segmental bone defects in sheep (Table 1, entry #16) [35].

$CoFe_2O_4$ nanoparticles have been used to reinforce the piezoelectric response of PVDF-TrFE membranes with microscale straight-stripe distribution of surface potential [36]. The straight-stripe distribution of charges notably improved the healing of skull bone defects compared to non-pattern membranes, which may be related to a facilitated cytoskeleton orientation and osteogenic differentiation (Table 1, entry #17).

Inorganic scaffolds based on GaN/AlGaN (with a negatively charged surface) are able to facilitate bone formation in critical defects even when there is a gap between the bone walls and the scaffold [37]. Negatively charged surfaces caused an upregulation of osteogenesis-related genes, although the mechanisms are still to be elucidated (Table 1, entry #18). Ceramics inspired in the ECM of bone have been made with $K_{0.5}Na_{0.5}NbO_3$ (KNN) that was selectively irradiated to mimic the ECM alternative domains of piezoelectric collagenous materials and non-piezoelectric non-collagenous materials [38]. The laser-irradiated microzones underwent a transition from mixed orthorhombic and tetragonal phases (highly piezoelectric) to a tetragonal solely phase (less piezoelectric). Mimicking the spatial distribution of the physiological electro-microenvironment of the bone, more efficient osteogenic differentiation and bone regeneration were observed. Despite the laser-irradiated KNN ceramic was less piezoelectric than the pristine ceramic, the former induced greater bone regeneration in a rabbit condyle bone defect model (Table 1, entry #19), revealing the importance of the spatial distribution of the piezoelectric domains.

5. Piezolectric scaffolds for tendon regeneration

Tendon cells are highly mechanosensitive. Their specialized sensory machinery includes mechanosensitive ion channels that are involved in the signaling pathways for repair [74]. Tendons connect muscle to bone and, thus, they are under repeated mechanical stress. The high mechanical stress can be supported thanks to the highly anisotropic extracellular matrix, which is mainly composed of type I collagen, an efficient piezoelectric material.

Scaffolds of collagen with aligned nanofibers of P(VDF-TrFE) have been tested *in vivo* to repair Achilles tendon acute injuries [17]. The nanofibers were collected on a disk rotating at a linear velocity of 29.3 m/s to align fibers of 390–540 nm in diameter, which is in the range of collagen fibers in tendon, and then post-processed to further increase the β-phase. A non-piezoelectric PTFE scaffold was used as a control to differentiate between stimulation due to mechanical load and to the piezoelectric stimulus. In cell culture, mechanically-induced piezoelectricity (0.5 Hz frequency and 4% strain) of P(VDF-TrFE) scaffold was shown to modulate ion channels and to significantly increase tenomodulin expression, without altering bone-related genes. Differently, mechanical stimulation of PTFE scaffold mainly induced a significant up-regulation of genes associated to bone differentiation. The relevance of electromechanical stimulation was confirmed *in vivo* in a full thickness rat Achilles acute tendon injury model, demonstrating the feasibility of modulation of expression of ion channels (TRPA1, PIEZO1/2, and KCNK2/4) and attenuation of bone morphogenetic protein (BMP) signaling associated to excessive bone growth (Table 2, entry #1).

6. Piezolectric scaffolds for nerve regeneration

Nerve regeneration is a particularly challenging clinical need as the damaged region lacks any tension for nerve reconstruction. A wide variety of strategies, such as donor grafting, decellularized nerve conduits, and synthetic scaffolds with and without stem cells, have shown so far limited success *in vivo* [95]. Externally applied electrical stimulation has demonstrated enhanced migration and proliferation of Schwann cells and faster nerve reinnervation, but invasive implantation of the electrical components limits the patient's daily activity and movement [39].

Piezoelectric materials appear as the most promising alternative for nerve repair avoiding the invasiveness of the devices that depend on external stimulation. Poly-ε-caprolactone (PCL) scaffolds with piezoelectric boron nitride nanosheets were demonstrated useful for the repair of a severe sciatic nerve lesion by promoting microvessel formation and reversing the muscular atrophy in animals that followed a daily treadmill running (Table 2, entry #2) [40]. Similarly, aligned electrospun fibers of PCL and ZnO have shown ability to shorten the reconnection time of damaged axons from 8 to 12 weeks with traditional treatment to 4 weeks, by providing biomimetic output voltages in the 40–120 mV (Fig. 8) [41]. ZnO was safe for Schwann cells up to concentrations of 0.63 mg/L, which means that nanofibers with up to 2% in ZnO can be considered biocompatible. Schwann cells, which are electrically sensitive cells, showed enhanced expression of nerve growth factor (NGF) and vascular epithelial growth factor (VEGF) after being cultured in the piezoelectric scaffold on a Flexcell tension system. Once implanted in the rat sciatic nerve defect (1.0 cm gap), the PCL-ZnO fibers notably improved both functional and morphological recovery in 28 days, compared to PCL solely fibers (Table 2, entry #3) [41].

Similarly, ZnO-loaded PCL scaffolds prepared using 3D injectable multilayer biofabrication notably favored the healing of sciatic nerve (1.5 cm gap) in a murine model when combined with physical exercise [91]. *In vitro* studies revealed that Schwann cells that were seeded on the ZnO/PCL scaffolds and stimulated using ultrasound (10 s, twice per day) showed enhanced attachment and proliferation compared to PCL scaffolds. The ZnO/PCL hybrid scaffolds implanted in the sciatic nerve gap notably accelerated the peripheral nerve regeneration and also promoted angiogenesis, particularly in animals that practice exercise during recovery **(Table 2, entry #3).**

PVDF-TrFE electrospun conduits have been shown to enhance noradrenergic axon regeneration after complete spinal cord transection [96]. The lesion was filled with Schwann cells and then the PVDF-TrFE electrospun conduit was used as a bridge between the rostral and the caudal stumps. After 3 weeks treatment, aligned conduits promoted the extension of $D\beta H^+$ (dopamine-beta-hydroxylase) axons and facilitated the growth of blood vessels through the transplant **(Table 2, entry #4)**.

For patients who lack mobility or with spinal cord injuries in which movement or exercise is forbidden, hybrid materials made of piezoelectric scaffolds and magnetic particles may significantly reinforce the healing output [42]. Magnetic stimulation of nanoparticles prepared with a core of Fe_3O_4 and a shell of $BaTiO_3$ ($d_{33} = 28$ pC/V) and dispersed in a hyaluronic acid/collagen hydrogel has been shown useful to enhance neurogenesis in a cell culture. Respiratory motion is also being explored as a source of mechanical stimuli for scaffolds implanted in thorax subcutaneous adipose tissue. Through an adequate design of PVDF/ZnO electrospun mats that were sandwiched in polydimethylsiloxane (PDMS), the electrical signal can reach nerve defects when connected to conduits prepared with conductive materials such as chitosan, PLLA and poly(3,4-ethylene dioxythiophene) (PEDOT) [97].

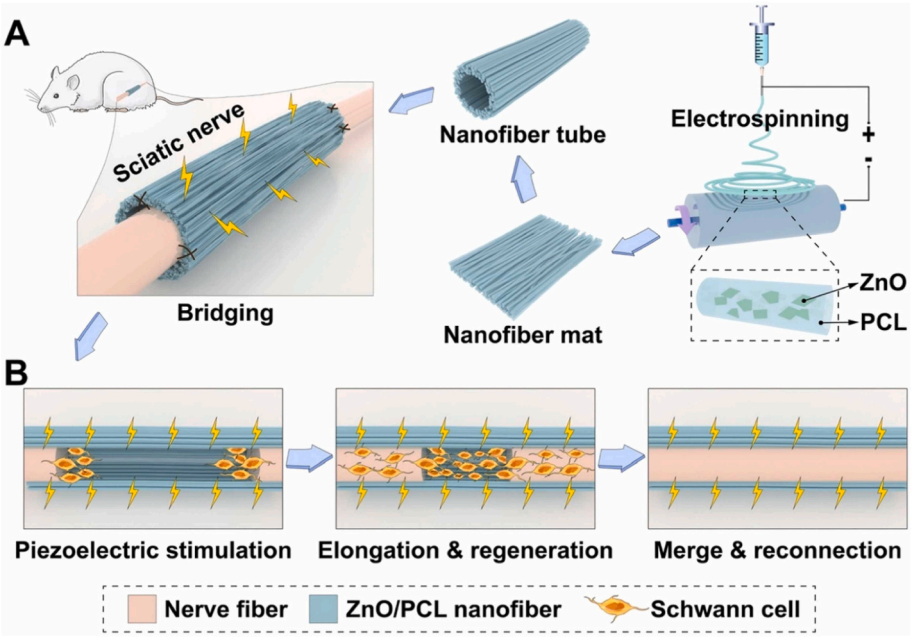

Fig. 8. (A) Conceptual design of an electrospun mat of PCL and ZnO that is wrapped into a nanofiber tube (0.5 mm in diameter) to act as a piezoelectric scaffold for rat sciatic nerve repair; and (B) once implanted, the piezoelectric stimulation provided by the scaffold favors Schwann cell recruitment and proliferation for a complete axon reconnection. Reproduced from Mao et al. [41] with permission of Elsevier.

Although this strategy is quite complex and involves several devices and surgeries, the feasibility of reconstruction of nerves that are far from the piezoelectric device and only stimulated by the breathing was demonstrated *in vivo* for 15 mm length nerve defects (Table 2, entry #5).

7. Piezolectric scaffolds for wound healing

A variety of wound dressings that can self-generate microelectric potentials are under investigation to both accelerate skin healing and prevent bacteria growth and biofilm development [98]. A pioneered representative is Procellera®, a wireless electroceutical dressing (WED) approved by FDA in 2013 [99], which contains silver (Ag) and zinc (Zn) separated from each other and generates an electrical field in the presence of a conductive liquid such as the wound fluid (Fig. 9A). 2D and 3D printing technologies may allow spatially controlled separation of Ag and Zn, obtaining microcircuits with microelectric potentials of 0.5–0.9 V, which remain stable when the device is exposed to an infection-mimicking environment [100]. The antimicrobial mechanism relies on a direct action of silver and zinc ions and the generation of ROS under an adequate redox potential, which is useful for thin infection layers [43]. Similarly, microneedles made of platinum–ruthenium nanoalloys and porous nanosheets of graphitic carbon nitride C_3N_5 have been shown useful for eradicating bacteria after 10 min ultrasound treatment, which accelerated the healing of infected wounds in a mouse model (Table 2, entry #6) [101]. Platinum–ruthenium nanoalloys perform as oxidase (OXD)-like nanozymes which convert oxygen molecules in the infected wounds into antimicrobial ROS, but with low performance. The piezoelectric field induced by ultrasound in the C_3N_5 nanosheets notably reinforced the production of ROS. Similar outcomes were reported for hydrogels loaded with C_3N_4 nanosheets that generate H_2 under ultrasound activation [44].

High production of ROS has also been recorded for $BaTiO_3$ nanocubes modified with gold nanoparticles (Au@$BaTiO_3$) when activated using ultrasound [45]. The piezoelectric composite was capable of eradicating Gram-negative *Escherichia coli* and Gram-positive *Staphylococcus aureus* bacteria by causing an intense lipid peroxidation of the cell membrane and subsequent intracellular protein leakage. Studies carried out in *S. aureus*-infected dermal wounds (mouse model) revealed the efficient bacteria killing effect of the combination of Au@$BaTiO_3$ and ultrasound, while promoting fibroblasts migration, collagen deposition and angiogenesis for wound healing (Table 2, entry #7). The efficacy of this approach was also demonstrated for conditions mimicking infections in deep tissues.

$BaTiO_3$ coated with a zeolitic imidazolate framework-8 (ZIF-8) and loaded with ciprofloxacin were dually responsive to ultrasound (piezoelectric response) and to pH, with an enhanced release rate of ciprofloxacin in an acidic environment [46]. The improved healing of infected wounds was attributed to the concomitant effects of piezoelectricity and Zn^{2+} ions (from ZIF-8 degradation) on cell migration, and of ROS generation and ciprofloxacin on inhibition of bacterial growth (Table 2, entry #8). Ultrasound irradiation was demonstrated to be a key factor for the fully development of the piezoelectric capability of these scaffolds, which in this case was a mass of nanoparticles that may fail to be activated by simple movement of the skin.

Similarly, piezoelectric $MoSe_2$ nanoflowers were shown to mimic glutathione oxidase and peroxidase activity, inducing high oxidative stress under ultrasound irradiation [102]. Ultrasound application enhanced the production of free radicals, which were strongly toxic for methicillin-resistant *S. aureus* biofilms both *in vitro* and *in vivo*, while wound healing was notably faster (Table 2, entry #9).

Piezoelectric polymers without inorganic particles have also demonstrated a huge potential to provide antimicrobial protection in a non-specific manner. Antibiotic-free PLLA films were designed to exhibit bactericidal properties against both Gram-positive *Staphylococcus epidermidis* and Gram-negative *E. coli* [47]. Compared to smooth films, nanotextured films showed higher crystallinity and stronger piezoelectric properties, which resulted in a more efficient bactericidal properties. Piezoelectricity was shown to damage the bacteria membrane causing content leakage while did not affect to the human red blood cells. Compared to inorganic materials, although the bactericidal mechanism is not fully elucidated, piezoelectric polymers have the advantage of triggering less ROS since their piezoelectric properties are not sufficient to hydrolyze water ($d_{33} > 100$ pC/N). Interestingly, vitamin B2 was recently found to increase the crystallinity and β-phase of piezoelectric polymers, such as PLLA, notably reinforcing the piezoelectric output [48]. Films of PLLA with vitamin B2 under ultrasound stimulation

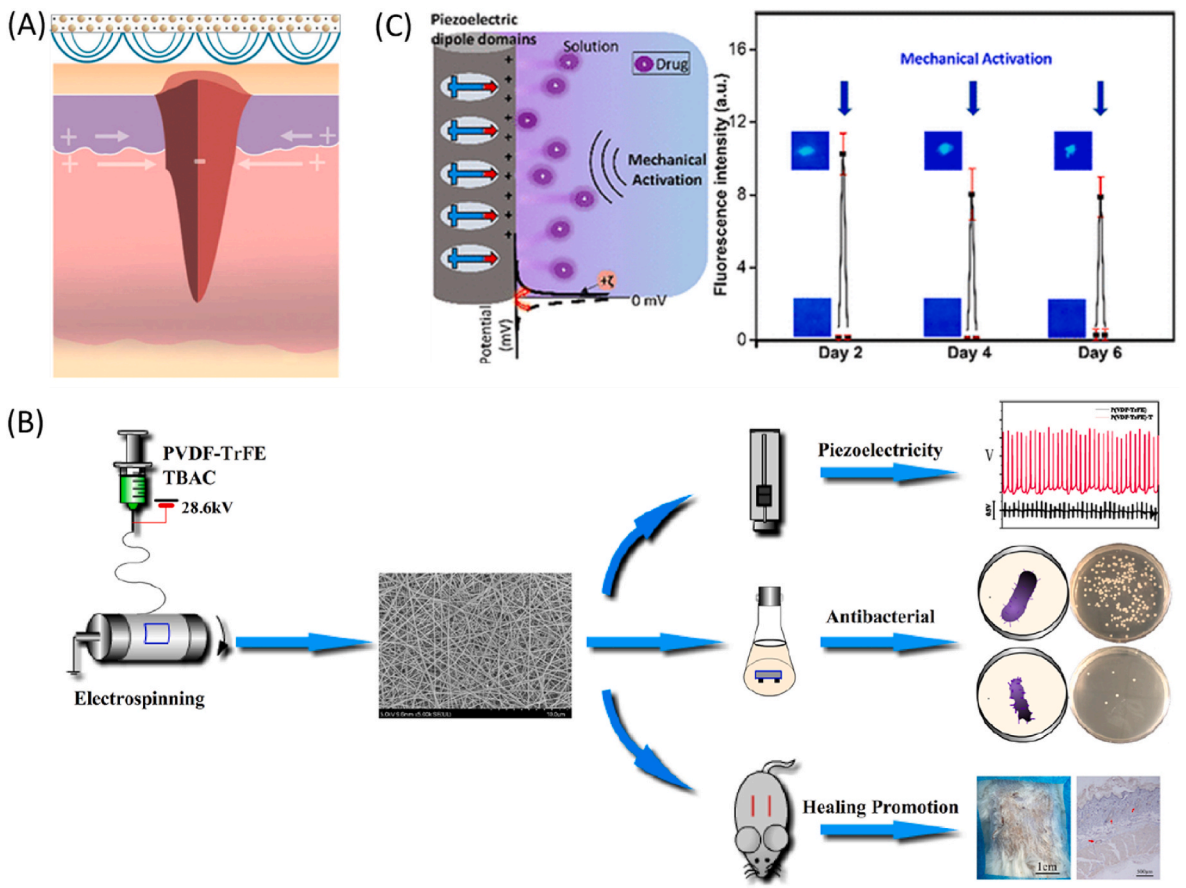

Fig. 9. (A) Scheme of a wound with a wireless electroceutical dressing (WED) on top. The dressing consists of a matrix of alternating Ag and Zn dots on a polyester substrate. The microcurrent of the WED is in the 2–10 μA range and aids in wound healing while exerts antimicrobial effects. Reproduced from Kim et al. [98] with permission of Oxford University Press. (B) P(VDF-TrFE) with tetrabutylammonium chloride (TBAC) electrospun mats showed reinforced piezoelectricity compared to fibers without TBAC, which in turn enhanced the antibacterial activity and the healing of deep skin wounds. Reproduced from Yang et al. [51] with permission of Springer Nature. (C) P(VDF-TrFE) nanofibers have negative zeta potential at rest which allows the loading of cationic drugs. Mechanical stimuli modify the surface charge and trigger drug release until the surface recovers the initial negative charge. Reprinter from Jariwala et al. [52] with permission from the American Chemical Society. Copyright© 2021 American Chemical Society.

notably enhanced cell migration and favored wound closure, through an increase in the expression of collagen, VEGF, epidermal growth factor (EGF) and fibroblast growth factor (FGF) (Table 2, entry #10).

Wound repair has also been accelerated with the application of piezoelectric poly(hydroxybutyrate-co-valerate) (PHBV) (1.3 pC/N) [49]. To counteract the hydrophobicity and poor cell adhesion properties of PHBV, electrospun fibers were prepared with mixtures of polydioxanone (PDX) covering a wide range of ratios. PDX/PHBV 20/80 mats were placed in full thickness wounds and notably enhanced the healing in terms of granulation tissue, thickness of stratum corneum and epidermis, compared to PDX solely mats (Table 2, entry #11). These findings highlight the interest of piezoelectric dressings to reconstruct fully functional skin.

Electrospun P(VDF-TeFE) nanofibers have also been designed for the treatment of oral wounds (palatal site lesions). Aligned nanofibers were collected using a cylindrical collector under rotation and then they were sputtered with copper to be endowed with antimicrobial properties (Table 2, entry #12). The mats were tested in oral mucosa lesion (7 × 4 mm) in a rat model against a control without any bandage. After 7 days of treatment, control wounds were infected and showed edema and necrosis. Differently, the animals treated with P(VDF-TeFE) mats with or without Cu showed a decrease in the size of the lesions, with abundant connective tissue and newly formed vessels. It was hypothesized that the mats protect the palatal surface from the mechanical friction caused by food, and at the same time the intake of food and water may act as a mechanical stimulus to generate piezoelectricity, which in turn favors cell migration and growth [50].

The antimicrobial features of piezoelectricity can be reinforced by adding an antiseptic to the electrospun mat. P(VDF-TrFE) with tetrabutylammonium chloride (TBAC) membranes have shown a 5.3-fold increase in output voltage compared to P(VDF-TrFE) membranes (because of an increase in the β phase) and higher bactericidal effect against *E. coli* (97.25% inhibition) and *S. aureus* (71.43% inhibition) (Fig. 9B) [51]. While at rest the membranes had no antibacterial properties, under mechanical stimulation *in vitro* both P(VDF-TrFE) and P(VDF-TrFE)/TBAC evidenced bactericidal capability. The piezoelectric response triggered the production of ROS, particularly $OH^{\cdot}$, which was more intense in the case of P(VDF-TrFE)/TBAC. Relevantly, the most piezoelectric membranes did not cause detrimental effects on human cells but enhanced the proliferation of fibroblasts. Moreover, in a rat wound model P(VDF-TrFE)/TBAC piezoelectric membranes accelerated the healing rate by ca. 37% compared to the control, and the wound was completely healed at day 7 (Table 2, entry #13). P(VDF-TrFE) nanofibers containing TBAC and Fe_3O_4 have recently been integrated in a wound dressing as the upper layer of the device, on top of a bioadhesive hydrogel containing catechol-grafted alginate and iron ions [103]. The bioadhesive hydrogel played the two-fold roles of a better transmission of the mechanical forces to induce piezoelectricity and of the generated electricity towards the wound. The two-layers wound dressing notably enhanced the expression of bFGF, PDGF, and VEGF, which led to faster

healing of large full-thickness wounds (Table 2, entry #14).

As a complementary strategy, P(VDF-TrFE) nanofibers have been shown able to provide pulses of drug release when mechanically stimulated. At rest the surface charge of the nanofibers is negative and thus can adsorb cationic drugs (Fig. 9C). A mechanical stimulus modifies the surface potential and triggers drug release, which stops when the stimulus ceases [52]. Although still not verified *in vivo*, this strategy may open new ways of delivering electrical and pharmacological inputs to the wounds.

Finally, dually functional films for piezoelectrical and photothermal therapy have been prepared by coating chitosan films with polydopamine, which endowed the films with its capability to absorb 808 nm NIR light and to generate a local increase of temperature. In a full-thickness wound model (rat) chitosan/polydopamine films demonstrated enhanced capability to up-regulate heat shock protein 90 (Hsp90) and hypoxia-inducible factor 1 α (HIF-1 α), which in turn promoted angiogenesis, collagen deposition and cell migration (Table 2, entry #15). Polydopamine reinforced the piezoelectric signal of chitosan films, and the synergic effects of piezoelectricity and thermal therapy on wound healing were evident [104].

8. Conclusions and future trends

Bioelectric fields are important guiding cues for cell migration and differentiation during tissue regeneration. Thus, mimicking these natural stimuli appears as a very promising tool for regenerative medicine. Compared to external devices that can supply artificial electric fields, piezoelectric scaffolds have the advantages of using natural mechanical forces to generate biomimetic output voltages in an autonomous way in the affected tissue, avoiding the implantation of complicate devices. All cells are susceptible to electric signals and, therefore, piezoelectric scaffolds appear to be suitable for regeneration of any tissue if the electric output is adequately adjusted. Also relevantly, a wide range of materials can be candidates to components of piezoelectric scaffolds. Natural (e.g., DNA, collagen) and synthetic (e.g., PVDF, PLLA) polymers that lack a center of symmetry generate dipole moments when deformed, which cause a net polarization on their surface. Deformations (mechanical stress) can be induced by the own traction forces of the adhered cells, physiological movements (breathing, heart beating), daily activities (moderate exercise) or the external application of ultrasound (if the patient or the affected tissue cannot move). Importantly, the design of piezoelectric scaffolds requires a highly aligned ordering of the polymers in a crystalline state to emit electric signals of sufficient intensity. In this regard, electrospinning of well-aligned nanofibers, annealing, and incorporation of inorganic (ZnO, $(Na,K)NbO_3$, $BaTiO_3$) and organic (vitamin B2) additives may notably enhance the piezoelectric performance.

The results obtained so far *in vivo* in a variety of animal models reveal the valuable performance of piezoelectric scaffolds in terms of bone, cartilage, nerve and skin regeneration. However, translation to the clinical arena still requires addressing (i) the lack of standardization in the experimental conditions used to measure the piezoelectricity (set up, applied load, ultrasound irradiation time and intensity), which make the comparison of scaffolds outcomes very difficult, and (ii) the identification and quantification of the mechanisms involved in the healing of each tissue, including the downstream second-messenger cascades. Promisingly, the observed positive effects on mammalian cell chemotaxis and secretion of relevant growth factors are accompanied by negative effects on microorganisms that infect the growing tissue or the scaffold itself, aiding the tissue healing by prevention of biofilm formation. Also relevantly, piezoelectric scaffolds may be endowed with additional functionalities such as light responsiveness or drug loading to obtain synergic regenerative effects by combination with photothermal and pharmacological therapies.

Declaration of competing interest

The authors declare that they have no known competing financial interests or personal relationships that could have appeared to influence the work reported in this paper.

Data availability

This is a review.

Acknowledgements

Funding: The work was supported by MCIN/AEI/10.13039/501100011033 [PID 2020-113881RB-I00], Spain, Xunta de Galicia [ED431C 2020/17], FEDER, and GLIOSILK Project funded by Instituto de Salud Carlos III (ISCIII) [AC19/00067] Cofinanciado FEDER, Spain. A. S-R acknowledges a PRE2021-098268 fellowship financed by MCIN/AEI/10.13039/501100011033 and FSE+. M.Z. was financed by GLIOSILK Project funded by Instituto de Salud Carlos III (ISCIII) [AC19/00067] Cofinanciado FEDER, Spain.

References

[1] United Nations. Ageing. https://www.un.org/en/global-issues/ageing; accessed May 2023.
[2] Population Reference Bureau. https://www.prb.org/resources/countries-with-the-oldest-populations-in-the-world/; accessed May 2023.
[3] World Population Ageing, United Nations, 2015 report, https://digitallibrary.un.org/record/826633. accessed May 2023.
[4] M. Roser, H. Ritchie, F. Spooner, Burden of disease, Published online at OurWorldInData.org, Retrieved from: https://ourworldindata.org/burden-of-disease, 2021. accessed May 2023.
[5] Bone and Joint Initiative USA, The Hidden Impact of Musculoskeletal Disorders on Americans, fourth ed. https://www.boneandjointburden.org/fourth-edition/about; accessed May 2023..
[6] G. Yang, B.B. Rothrauff, R.S. Tuan, Tendon and ligament regeneration and repair: clinical relevance and developmental paradigm, Birth Defects Res. C Embryo Today. 99 (2013) 203–222.
[7] G.M. Hobusch, J. Bollmann, S.E. Puchner, N.W. Lang, J.G. Hofstaetter, P. T. Funovics, R. Windhager, What sport activity levels are achieved in patients after resection and endoprosthetic reconstruction for a proximal femur bone sarcoma? Clin. Orthop. Relat. Res. 475 (2017) 817–826.
[8] M. Olsson, K. Järbrink, U. Divakar, R. Bajpai, Z. Upton, A. Schmidtchen, J. Car, The humanistic and economic burden of chronic wounds: a systematic review, Wound Repair Regen. 27 (2019) 114–125.
[9] C. Alvarez-Lorenzo, C.A. Garcia-Gonzalez, E. Bucio, A. Concheiro, Stimuli-responsive polymers for antimicrobial therapy: drug targeting, contact-killing surfaces and competitive release, Expet Opin. Drug Deliv. 13 (2016) 1109–1119.
[10] S.J. Hollister, C.L. Flanagan, D.A. Zopf, R.J. Morrison, H. Nasser, J.J. Patel, E. Ebramzadeh, S.N. Sangiorgio, M.B. Wheeler, G.E. Green, Design control for clinical translation of 3D printed modular scaffolds, Ann. Biomed. Eng. 43 (2015) 774–786.
[11] Z. Fu, Y. Zhuang, J. Cui, R. Sheng, H. Tomás, J. Rodrigues, B. Zhao, X. Wang, K. Lin, Development and challenges of cells- and materials-based tooth regeneration, Eng. Regen. 3 (2022) 163–181.
[12] B. Tandon, J.J. Blaker, S.H. Cartmell, Piezoelectric materials as stimulatory biomedical materials and scaffolds for bone repair, Acta Biomater. 73 (2018) 1–20.
[13] C. Alvarez-Lorenzo, A. Concheiro, Smart drug release from medical devices, J. Pharmacol. Exp. Therapeut. 370 (2019) 544–554.
[14] R.R. Castillo, D. Lozano, B. González, M. Manzano, I. Izquierdo-Barba, M. Vallet-Regí, Advances in mesoporous silica nanoparticles for targeted stimuli-responsive drug delivery: an update, Expet Opin. Drug Deliv. 16 (2019) 415–439.
[15] P. Lavrador, V.M. Gaspar, J.F. Mano, Stimuli-responsive nanocarriers for delivery of bone therapeutics – barriers and progresses, J. Contr. Release 273 (2018) 51–67.
[16] G. Nourissat, F. Berenbaum, D. Duprez, Tendon injury: from biology to tendon repair, Nat. Rev. Rheumatol. 11 (2015) 223.
[17] M.A. Fernandez-Yague, A. Trotier, S. Demir, S.A. Abbah, A. Larrañaga, A. Thirumaran, A. Stapleton, S.A.M. Tofail, M. Palma, M. Kilcoyne, A. Pandit, M. J. Biggs, A self-powered piezo-bioelectric device regulates tendon repair-associated signaling pathways through modulation of mechanosensitive ion channels, Adv. Mater. 33 (2021), 2008788.
[18] R.H.W. Funk, Endogenous electric fields as guiding cue for cell migration, Front. Physiol. 6 (2015) 143.
[19] M.M. Balach, C.H. Casale, A.N. Campetelli, Erythrocyte plasma membrane potential: past and current methods for its measurement, Biophys Rev 11 (2019) 995–1005.

[20] H.F. Guo, Z.S. Li, S.W. Dong, W.J. Chen, L. Deng, Y.F. Wang, D.J. Ying, Piezoelectric PU/PVDF electrospun scaffolds for wound healing applications, Colloids Surf., B 96 (2012) 29–36.

[21] C. Ribeiro, D.M. Correia, I. Rodrigues, L. Guardão, S. Guimarães, R. Soares, S. Lanceros-Méndez, In vivo demonstration of the suitability of piezoelectric stimuli for bone reparation, Mater. Lett. 209 (2017) 118–121.

[22] C. Zhang, W. Liu, C. Cao, F. Zhang, Q. Tang, S. Ma, J. Zhao, L. Hu, Y. Shen, L. Chen, Modulating surface potential by controlling the β phase content in poly (vinylidene fluoridetrifluoroethylene) membranes enhances bone regeneration, Adv. Healthc. Mater. 7 (2018), 1701466.

[23] A. Wang, Z. Liu, M. Hu, C. Wang, X. Zhang, B. Shi, Y. Fan, Y. Cui, Z. Li, K. Ren, Piezoelectric nanofibrous scaffolds as in vivo energy harvesters for modifying fibroblast alignment and proliferation in wound healing, Nano Energy 43 (2018) 63–71.

[24] E.N. Bolbasov, D.A. Popkov, N.A. Kononovich, E.N. Gorbach, I.A. Khlusov, A. S. Golovkin, K.S. Stankevich, V.P. Ignatov, V.M. Bouznik, Y.G. Anissimov, S. I. Tverdokhlebov, A.V. Popkov, Flexible intramedullary nails for limb lengthening: a comprehensive comparative study of three nails types, Biomed. Mater. 14 (2019), 025005.

[25] J. Wu, T. Chen, Y. Wang, J. Bai, C. Lao, M. Luo, M. Chen, W. Peng, W. Zhi, J. Weng, J. Wang, Piezoelectric effect of antibacterial biomimetic hydrogel promotes osteochondral defect repair, Biomedicines 10 (2022) 1165.

[26] P. Chen, C. Xu, P. Wu, K. Liu, F. Chen, Y. Chen, H. Dai, Z. Luo, Wirelessly powered electrical-stimulation based on biodegradable 3d piezoelectric scaffolds promotes the spinal cord injury repair, ACS Nano 16 (2022) 16513–16528.

[27] R. Das, E.J. Curry, T.T. Le, G. Awale, Y. Liu, S. Li, J. Contreras, C. Bednarz, J. Millender, X. Xin, D. Rowe, S. Emadi, K.W.H. Lo, T.D. Nguyen, Biodegradable nanofiber bone-tissue scaffold as remotely-controlled and self-powering electrical stimulator, Nano Energy 76 (2020), 105028.

[28] Y. Liu, G. Dzidotor, T.T. Le, T. Vinikoor, K. Morgan, E.J. Curry, R. Das, A. McClinton, E. Eisenberg, L.N. Apuzzo, K.T.M. Tran, P. Prasad, T.J. Flanagan, S. W. Lee, H.M. Kan, M.T. Chorsi, K.W.H. Lo, C.T. Laurencin, T.D. Nguyen, Exercise-induced piezoelectric stimulation for cartilage regeneration in rabbits, Sci. Transl. Med. 14 (2022), eabi7282.

[29] X. Dai, X. Yao, W. Zhang, H. Cui, Y. Ren, J. Deng, X. Zhang, The osteogenic role of barium titanate/polylactic acid piezoelectric composite membranes as guiding membranes for bone tissue regeneration, Int. J. Nanomed. 17 (2022) 4339–4353.

[30] T. Zheng, Y. Yu, Y. Pang, D. Zhang, Y. Wang, H. Zhao, X. Zhang, H. Leng, X. Yang, Q. Cai, Improving bone regeneration with composites consisting of piezoelectric poly(l-lactide) and piezoelectric calcium/manganese co-doped barium titanate nanofibers, Compos. B Eng. 234 (2022), 109734.

[31] X. Zhang, C. Zhang, Y. Lin, P. Hu, Y. Shen, K. Wang, S. Meng, Y. Chai, X. Dai, X. Liu, Y. Liu, X. Mo, C. Cao, S. Li, X. Deng, L. Chen, Nanocomposite membranes enhance bone regeneration through restoring physiological electric microenvironment, ACS Nano 10 (2016) 7279–7286.

[32] H. Liu, Y. Shi, Y. Zhu, P. Wu, Z. Deng, Q. Dong, M. Wu, L. Cai, Bioinspired piezoelectric periosteum to augment bone regeneration via synergistic immunomodulation and osteogenesis, ACS Appl. Mater. Interfaces 15 (2023) 12273–12293.

[33] W. Liu, X. Li, Y. Jiao, C. Wu, S. Guo, X. Xiao, X. Wei, J. Wu, P. Gao, N. Wang, Y. Lu, Z. Tang, Q. Zhao, J. Zhang, Y. Tang, L. Shi, Z. Guo, Biological effects of a three-dimensionally printed Ti6Al4V scaffold coated with piezoelectric BaTiO3 nanoparticles on bone formation, ACS Appl. Mater. Interfaces 12 (2020) 51885–51903.

[34] B. Fan, Z. Guo, X. Li, S. Li, P. Gao, X. Xiao, J. Wu, C. Shen, Y. Jiao, W. Hou, Electroactive barium titanate coated titanium scaffold improves osteogenesis and osseointegration with low-intensity pulsed ultrasound for large segmental bone defects, Bioact. Mater. 5 (2020) 1087–1101.

[35] W. Liu, D. Yang, X. Wei, S. Guo, N. Wang, Z. Tang, Y. Lu, Z. Guo, Fabrication of piezoelectric porous BaTiO3 scaffold to repair large segmental bone defect in sheep, J. Biomater. Appl. 35 (2020) 544–552.

[36] J. Zhang, X. He, S. Lin, X. Chen, L. Dong, J. Lin, H. Wang, W. Weng, K. Cheng, Accelerated osteogenesis of heterogeneous electric potential gradient on CFO/P (VDF-TrFE) membranes, Adv. Mater. Interfac. 9 (2022), 2102549.

[37] C. Zhang, W. Wang, X. Hao, Y. Peng, Y. Zheng, J. Liu, Y. Kang, F. Zhao, Z. Luo, J. Guo, B. Xu, L. Shao, G. Li, A novel approach to enhance bone regeneration by controlling the polarity of GaN/AlGaN heterostructures, Adv. Funct. Mater. 31 (2021), 2007487.

[38] P. Yu, C. Ning, Y. Zhang, G. Tan, Z. Lin, S. Liu, X. Wang, H. Yang, K. Li, X. Yi, Y. Zhu, C. Mao, Bone-inspired spatially specific piezoelectricity induces bone regeneration, Theranostics 7 (2017) 3387–3397.

[39] M.P. Willand, M.A. Nguyen, G.H. Borschel, T. Gordon, Electrical stimulation to promote peripheral nerve regeneration, Neurorehabil, Neural Repair 30 (2016) 490–496.

[40] Y. Qian, Y. Xu, Z. Yan, Y. Jin, X. Chen, W.E. Yuan, C. Fan, Boron nitride nanosheets functionalized channel scaffold favors microenvironment rebalance cocktail therapy for piezocatalytic neuronal repair, Nano Energy 83 (2021), 105779.

[41] R. Mao, B. Yu, J. Cui, Z. Wang, X. Huang, H. Yu, K. Lin, S.G.F. Shen, Piezoelectric stimulation from electrospun composite nanofibers for rapid peripheral nerve regeneration, Nano Energy 98 (2022), 107322.

[42] Y. Zhang, S. Chen, Z. Xiao, X. Liu, C. Wu, K. Wu, A. Liu, D. Wei, J. Sun, L. Zhou, H. Fan, Magnetoelectric nanoparticles incorporated biomimetic matrix for wireless electrical stimulation and nerve regeneration, Adv. Healthc. Mater. 10 (2021), 2100695.

[43] H. Kim, I. Makin, J. Skiba, A. Ho, G. Housler, A. Stojadinovic, M. Izadjoo, Antibacterial efficacy testing of a bioelectric wound dressing against clinical wound pathogens, Open Microbiol. J. 8 (2014) 15–21.

[44] Q. Xu, S. Chen, L. Jiang, C. Xia, L. Zeng, X. Cai, Z. Jin, S. Qin, W. Ding, Q. He, Sonocatalytic hydrogen/hole-combined therapy for anti-biofilm and infected diabetic wound healing, Natl. Sci. Rev. 10 (2023) nwad063.

[45] M. Wu, Z. Zhang, Z. Liu, J. Zhang, Y. Zhang, Y. Ding, T. Huang, D. Xiang, Z. Wang, Y. Dai, X. Wan, S. Wang, H. Qian, Q. Sun, L. Li, Piezoelectric nanocomposites for sonodynamic bacterial elimination and wound healing, Nano Today 37 (2021), 101104.

[46] Z. Zhu, X. Gou, L. Liu, T. Xia, J. Wang, Y. Zhang, C. Huang, W. Zhi, R. Wang, X. Li, S. Luo, Dynamically evolving piezoelectric nanocomposites for antibacterial and repair-promoting applications in infected wound healing, Acta Biomater. 157 (2023) 566–577.

[47] L. Gazvoda, M.P. Nanut, Ma Spreitzer, M. Vukomanović, Antimicrobial activity of piezoelectric polymer: piezoelectricity as the reason for damaging bacterial membrane, Biomater. Sci. 10 (2022) 4933.

[48] Z. Zhang, L. Wang, Q. Zhang, H. Li, Y. Xiang, X. Wang, X. Hu, Effective electrical stimulation by a poly(l-lactic acid)/vitamin B2-based piezoelectric generator promotes wound healing, Eur. Polym. J. 189 (2023), 111962.

[49] N. Goonoo, F. Gimié, I. Ait-Arsa, C. Cordonin, J. Andries, D. Jhurry, A. Bhaw-Luximon, Piezoelectric core–shell PHBV/PDX blend scaffolds for reduced superficial wound contraction and scarless tissue regeneration, Biomater. Sci. 9 (2021) 5259–5274.

[50] A.D. Badaraev, A. Koniaeva, S.A. Krikova, E.V. Shesterikov, E.N. Bolbasov, A. L. Nemoykina, V.M. Bouznik, K.S. Stankevich, Y.M. Zhukov, I.P. Mishin, E. Y. Varakuta, S.I. Tverdokhlebov, Piezoelectric polymer membranes with thin antibacterial coating for the regeneration of oral mucosa, Appl. Surf. Sci. 504 (2020), 144068.

[51] N. Yang, Y. Chen, N. Dan, X. Zheng, R. Feng, G. Yu, X. He, W. Dan, Y. Wang, Flexible nano-piezoelectric membranes with spontaneous electric field generation for bacteria elimination and wound healing, J. Mater. Sci. 57 (2022) 19532–19552.

[52] T. Jariwala, G. Ico, Y. Tai, H. Park, N.V. Myung, J. Nam, Mechano-responsive piezoelectric nanofiber as an on-demand drug delivery vehicle, ACS Appl. Bio Mater. 4 (2021) 3706–3715.

[53] L. Chung, D.R. Maestas Jr., F. Housseau, J.H. Elisseeff, Key players in the immune response to biomaterial scaffolds for regenerative medicine, Adv. Drug Deliv. Rev. 114 (2017) 184–192.

[54] C.J. Wilson, R.E. Clegg, D.I. Leavesley, M.J. Pearcy, Mediation of biomaterial-cell interactions by adsorbed proteins: a review, Tissue Eng. 11 (2005) 1–18.

[55] A. Vishwakarma, N.S. Bhise, M.B. Evangelista, J. Rouwkema, M.R. Dokmeci, A. M. Ghaemmaghami, N.E. Vrana, A. Khademhosseini, Engineering immunomodulatory biomaterials to tune the inflammatory response, Trends Biotechnol. 34 (2016) 470–482.

[56] E. Mariani, G. Lisignoli, R.M. Borzì, L. Pulsatelli, Biomaterials: foreign bodies or tuners for the immune response? Int. J. Mol. Sci. 20 (2019) 636.

[57] U. Meyer, A. Buchter, H.P. Wiesmann, U. Joos, D.B. Jones, Basic reactions of osteoblasts on structured material surfaces, Eur. Cell. Mater. 9 (2005) 39–49.

[58] H.J. Kim, U.J. Kim, G. Vunjak-Novakovic, B.H. Min, D.L. Kaplan, Influence of macroporous protein scaffolds on bone tissue engineering from bone marrow stem cells, Biomaterials 26 (2005) 4442–4452.

[59] D.R. Albrecht, G.H. Underhill, T.B. Wassermann, R.L. Sah, S.N. Bhatia, Probing the role of multicellular organization in three-dimensional microenvironments, Nat. Methods 3 (2006) 369–375.

[60] A. Rosenthal, A. Macdonald, J. Voldman, Cell patterning chip for controlling the stem cell microenvironment, Biomaterials 28 (2007) 3208–3216.

[61] M. Levin, Reprogramming cells and tissue patterning via bioelectrical pathways: molecular mechanisms and biomedical opportunities, WIREs Syst. Biol. Med. 5 (2013) 657–676.

[62] M. Levin, Bioelectric mechanisms in regeneration: unique aspects and future perspectives, Semin. Cell Dev. Biol. 20 (2009) 543–556.

[63] M.A. Messerli, D.M. Graham, Extracellular electrical fields direct wound healing and regeneration, Biol. Bull. 221 (2011) 79–92.

[64] M. Yang, W.J. Brackenbury, Membrane potential and cancer progression, Front. Physiol. 4 (2013) 185.

[65] S. Sundelacruz, M. Levin, D.L. Kaplan, Membrane potential controls adipogenic and osteogenic differentiation of mesenchymal stem cells, PLoS One 3 (2008) e3737.

[66] L. Zhan, A. Rosenberg, K.C. Bergami, M. Yu, Z. Xuan, A.B. Jaffe, C. Allred, S. K. Muthuswamy, Deregulation of Scribble promotes mammary tumorigenesis and reveals a role for cell polarity in carcinoma, Cell 135 (2008) 865–878.

[67] A. Pietak, M. Levin, Bioelectrical control of positional information in development and regeneration: a review of conceptual and computational advances, Prog. Biophys. Mol. Biol. 137 (2018) 52–68.

[68] L. Abdul Kadir, M. Stacey, R. Barrett-Jolley, Emerging roles of the membrane potential: action beyond the action potential, Front. Physiol. 9 (2018) 1661.

[69] D. Iandolo, A. Ravichandran, X. Liu, F. Wen, J.K.Y. Chan, M. Berggren, S.H. Teoh, D.T. Simon, Development and characterization of organic electronic scaffolds for bone tissue engineering, Adv. Healthc. Mater. 5 (2016) 1505–1512.

[70] E.P. e Silva, B. Huang, J.V. Helaehil, P.R.L. Nalesso, L. Bagne, M.A. de Oliveira, G. C.C. Albiazetti, A. Aldalbahi, M. El-Newehy, M. Santamaria Jr., F.A.S. Mendonça, P. Bártolo, G.F. Caetano, In vivo study of conductive 3D printed PCL/MWCNTs scaffolds with electrical stimulation for bone tissue engineering, Bio-Des. Manuf. 4 (2021) 190–202.

[71] D. Khare, B. Basu, A.K. Dubey, Electrical stimulation and piezoelectric biomaterials for bone tissue engineering applications, Biomaterials 258 (2020), 12028.
[72] K. Kapat, Q.T.H. Shubhra, M. Zhou, S. Leeuwenburgh, Piezoelectric nano-biomaterials for biomedicine and tissue regeneration, Adv. Funct. Mater. 30 (2020), 1909045.
[73] P. Delmas, T. Parpaite, B. Coste, PIEZO channels and newcomers in the mammalian mechanosensitive ion channel family, Neuron 110 (2022) 2713–2727.
[74] A. Savadipour, D. Palmer, E.V. Ely, K.H. Collins, J.M. Garcia-Castorena, Z. Harissa, Y. Seon Kim, A. Oestreich, F. Qu, N. Rashidi, F. Guilak, The role of PIEZO ion channels in the musculoskeletal system, Am. J. Physiol. Cell Physiol. 324 (2023) C728–C740.
[75] P. Poillot, J. O'Donnell, D.T. O'Connor, E.U. Haq, C. Silien, S.A.M. Tofail, J. M. Huyghe, Piezoelectricity in the intervertebral disc, J. Biomech. 102 (2020), 109622.
[76] A.H. Rajabi, M. Jaffe, T.L. Arienzeh, Piezoelectric materials for tissue regeneration: a review, Acta Biomater. 24 (2015) 12–23.
[77] N. Goonoo, A. Bhaw-Luximon, Piezoelectric polymeric scaffold materials as biomechanical cellular stimuli to enhance tissue regeneration, Mater. Today Commun. 31 (2022), 103491.
[78] M. Minary-Jolandan, M.F. Yu, Uncovering nanoscale electromechanical heterogeneity in the subfibrillar structure of collagen fibrils responsible for the piezoelectricity of bone, ACS Nano 3 (2009) 1859–1863.
[79] C. Halperin, S. Mutchnik, A. Agronin, M. Molotskii, P. Urenski, M. Salai, G. Rosenman, Piezoelectric effect in human bones studied in nanometer scale, Nano Lett. 4 (2004) 1253–1256.
[80] Y. Tang, C. Wu, Z. Wu, L. Hu, W. Zhang, K. Zhao, Fabrication and in vitro biological properties of piezoelectric bioceramics for bone regeneration, Sci. Rep. 7 (2017), 43360.
[81] A.C. Ahn, A.J. Grodzinsky, Relevance of collagen piezoelectricity to "Wolff's Law": a critical review, Med. Eng. Phys. 31 (2009) 733–741.
[82] T. Kubo, Piezoelectricity of bone and electrical callus, J. Orthop. Sci. 17 (2012) 105–106.
[83] D. Lacroix, P.J. Prendergast, A mechano-regulation model for tissue differentiation during fracture healing: analysis of gap size and loading, J. Biomech. 35 (2002) 1163–1171.
[84] G. Xia, B. Song, J. Fang, Electrical stimulation enabled via electrospun piezoelectric polymeric nanofibers for tissue regeneration, Research 2022 (2022), 9896274.
[85] Z. Ma, X. Hu, Y. Zhang, X. Li, B. Chen, Q. An, Y. Zhao, Y. Zhang, Biomineralized piezoelectrically active scaffolds for inducing osteogenic differentiation, Chemistry 29 (2023), e202203166.
[86] J. Jacob, N. More, K. Kalia, G. Kapusetti, Piezoelectric smart biomaterials for bone and cartilage tissue engineering, Inflamm. Regen. 38 (2018) 2.
[87] Y. Ikada, Y. Shikinami, Y. Hara, M. Tagawa, E. Fukada, Enhancement of bone formation by drawn poly(L-lactide), J. Biomed. Mater. Res. 30 (1996) 553–558.
[88] C.S. Lovell, J.M. Fitz-Gerald, C. Park, Decoupling the effects of crystallinity and orientation on the shear piezoelectricity of polylactic acid, J. Polym. Sci., Part B: Polym. Phys. 49 (2011) 1555–1562.
[89] T. Yucel, P. Cebe, D.L. Kaplan, Structural origins of silk piezoelectricity, Adv. Funct. Mater. 21 (2011) 779–785.
[90] Q. Liu, S. Xie, D. Fan, T. Xie, G. Xue, X. Gou, X. Li, Integrated osteochondral differentiation of mesenchymal stem cells on biomimetic nanofibrous mats with cell adhesion-generated piezopotential gradients, Nanoscale 14 (2022) 3865.
[91] Y. Qian, Y. Cheng, J. Song, Y. Xu, W.E. Yuan, C. Fan, X. Zheng, Mechano-informed biomimetic polymer scaffolds by incorporating self-powered zinc oxide nanogenerators enhance motor recovery and neural function, Small 16 (2020), 2000796.
[92] M.S. Ramasamy, V.K. Kaliannagounder, A. Rahaman, C.H. Park, C.S. Kim, B. Kim, Synergistic effect of reinforced multiwalled carbon nanotubes and boron nitride nanosheet-based hybrid piezoelectric PLLA scaffold for efficient bone tissue regeneration, ACS Biomater. Sci. Eng. 8 (2022) 3542–3556.
[93] Y. Zhang, L. Chen, J. Zeng, K. Zhou, D. Zhang, Aligned porous barium titanate/hydroxyapatite composites with high piezoelectric coefficients for bone tissue engineering, Mater. Sci. Eng. C 39 (2014) 143–149.
[94] X. He, E. Obeng, X. Sun, N. Kwon, J. Shen, J. Yoon, Polydopamine, harness of the antibacterial potentials-A review, Materials Today Bio 15 (2022), 100329.
[95] C.R. Carvalho, J.M. Oliveira, R.L. Reis, Modern trends for peripheral nerve repair and regeneration: beyond the hollow nerve guidance conduit, Front. Bioeng. Biotechnol. 7 (2019) 337.
[96] Y.S. Lee, S. Wu, T.L. Arinzeh, M.B. Bunge, Enhanced noradrenergic axon regeneration into Schwann cell-filled PVDF-TrFE conduits after complete spinal cord transection, Biotechnol. Bioeng. 114 (2017) 444–456.
[97] F. Jin, T. Li, T. Yuan, L. Du, C. Lai, Q. Wu, Y. Zhao, F. Sun, L. Gu, T. Wang, Z.-Q. Feng, Physiologically self-regulated, fully implantable, battery-free system for peripheral nerve restoration, Adv. Mater. 33 (2021), 2104175.
[98] H. Kim, S. Park, G. Housler, V. Marcel, S. Cross, M. Izadjoo, An overview of the efficacy of a next generation electroceutical wound care device, Mil. Med. 181 (2016) 184–190.
[99] https://www.accessdata.fda.gov/cdrh_docs/pdf13/k130350.pdf.
[100] S.S. Park, H. Kim, I.R.S. Makin, J.B. Skiba, M.J. Izadjoo, Measurement of microelectric potentials in a bioelectrically-active wound care device in the presence of bacteria, J. Wound Care 24 (2015) 23–33.
[101] S. Shi, Y. Jiang, Y. Yu, M. Liang, Q. Bai, L. Wang, D. Yang, N. Sui, Z. Zhu, Piezo-augmented and photocatalytic nanozyme integrated microneedles for antibacterial and anti-inflammatory combination therapy, Adv. Funct. Mater. 33 (2022), 2210850.
[102] X. Gao, Y. Liu, Y. Li, B. Jin, P. Jiang, X. Chen, C. Wei, J. Sheng, Y.N. Liu, J. Li, W. Chen, Piezoelectric nanozyme for dual-driven catalytic eradication of bacterial biofilms, ACS Appl. Mater. Interfaces 15 (2023) 14690–14703.
[103] Y. Chen, W. Xu, X. Zheng, X. Huang, N. Dan, M. Wang, Y. Li, Z. Li, W. Dan, Y. Wang, Two-layered biomimetic flexible self-powered electrical stimulator for promoting wound healing, Biomacromolecules 24 (2023) 1483–1496.
[104] Y. Chen, M. Ye, L. Song, J. Zhang, Y. Yang, S. Luo, M. Lin, Q. Zhang, S. Li, Y. Zhou, A. Chen, Y. An, W. Huang, T. Xuan, Y. Gu, H. He, J. Wu, X. Li, Piezoelectric and photothermal dual functional film for enhanced dermal wound regeneration via upregulation of Hsp90 and HIF-1 α, Appl. Mater. Today 20 (2020), 100756.